The Hebrew University of Jerusalem,

the Faculty of Mathematics and

Sciences

Department of Applied Physics

Soliton shedding from Airy pulse in Kerr media

Written by: Yiska Fattal,

021682554

Advisor: Dr. Dan Marom

Master thesis in sciences

Presented at: May 2012

Abstract

An Airy pulse, a solution of the dispersion equation, manifests two unique properties while propagating in linear media. One is self-similarity, meaning the pulse has the same envelope throughout propagation in dispersive media and the second is acceleration in time- namely moving in parabolic trajectory with respect to a time frame that moves with the group velocity of the pulse.

We simulate and analyze the propagation of truncated temporal Airy pulses in a single mode fiber in the presence of self-phase modulation (Kerr effect) and anomalous dispersion. Due to the presence of the nonlinear effect, the Airy is no longer a valid solution, such that the pulse evolution is no more predictable.

By gradually increasing the launched Airy power we examine the nonlinearity influence on the Airy pulse evolution. For sufficient large launched intensity we observe soliton pulse shedding from the Airy main lobe, with the emergent soliton parameters dependent on the launched Airy pulse characteristics. The emergent soliton performs "breathing"- periodic oscillations of its parameters along the propagation distance due to interaction with background radiation, with the periodicity increasing with the launched power. Additionally, the soliton mean temporal position shifts to earlier times with higher launched powers due to an earlier shedding event and with greater energy in the Airy tail due to collisions with the accelerating lobes. In spite of the Airy energy loss to the shed Soliton, the Airy pulse continues to exhibit the unique property of acceleration in time and the main lobe recovers from the energy loss (healing property of Airy waveforms), but performs decaying oscillations of its peak power according to the interplay between the dispersion and the nonlinear effect.

The influence of the truncation coefficient—required for limiting the Airy pulse to finite energy—on the Airy nonlinear propagation is also investigated. Small truncation degree increases the Airy tail energy, which has considerable influence on the soliton shedding distance, the soliton mean temporal position, and on the residual accelerating energy.

Table of content:

Abstract **2**

1 Theoretical background **4**

1.1 Dispersion phenomena *4*

1.2 Nonlinear phenomena in fibers *5*

1.3 The pulse propagation equation *7*

1.3.1 Dispersion-induced pulse broadening 9

1.3.2 SPM-Induced Spectral Broadening 11

1.3.3 Effect of Group-Velocity Dispersion with Self-Phase Modulation 14

1.4 The Airy pulse *16*

1.5 The soliton pulse *19*

2 Goals **22**

3 Methods- Numerical Simulation for pulse propagation **23**

3.1 Introduction to the Split Step Fourier method *23*

3.2 The algorithm *24*

3.3 Consideration and limitations *25*

4 Airy propagation in nonlinear media- simulations result and analysis **28**

4.1 Effects of launched Airy power *28*

4.2 Truncation coefficient effect *33*

4.3 Soliton time position for power and truncation *37*

4.4 Preliminary results of higher launched power Airy propagation *38*

5 Discussion and summary **41**

6 References **42**

7 Appendix **44**

7.1 Appendix A- Matlab code *44*

7.2 Appendix B- published paper *47*

1 Theoretical background

In this thesis we deal with pulse propagation in silica fiber, where the dispersion phenomena and the nonlinear phenomena dominate and influence the pulse evolution during the propagation. In this section we will discuss in detail these two phenomena and how they influence the pulse propagation. Then we will introduce two special pulses- Airy pulse and soliton pulse, whose propagation is investigated in this thesis. Except for the sub-section that deals with the Airy pulse, this section is based on the book "Nonlinear Fiber Optics", written by G.P. Agrawal [1].

1.1 Dispersion phenomena

When an electromagnetic wave interacts with the bound electrons of a dielectric, the medium response, in general, depends on the optical frequency ω. This property, referred to as chromatic dispersion, manifests through the frequency dependence of the refractive index $n(\omega)$. Fiber dispersion plays a critical role in propagation of short optical pulses because different spectral components associated with the pulse travel at different speeds given by $c/n(\omega)$.

Mathematically, the effects of fiber dispersion are accounted for by expanding the mode-propagation constant β in a Taylor series about the frequency ω_0 at which the pulse spectrum is centered:

$$\beta(\omega) = n(\omega)\frac{\omega}{c} = \beta_0 + \beta_1(\omega-\omega_0) + \beta_2(\omega-\omega_0)^2 + ... \qquad \textbf{1.1}$$

where

$$\beta_m = \left(\frac{d^m\beta}{d\omega^m}\right)_{\omega=\omega_0}, m = 0,1,2.... \qquad \textbf{1.2}$$

The parameters β_1 and β_2 are related to the refractive index n and its derivatives through the relations

$$\beta_1 = \frac{1}{v_g} = \frac{n_g}{c} = \frac{1}{c}\left(n + \omega\frac{dn}{d\omega}\right), \beta_2 = \frac{1}{c}\left(2\frac{dn}{d\omega} + \omega\frac{d^2n}{d\omega^2}\right) \qquad \textbf{1.3}$$

where n_g is the group index and v_g is the group velocity. Physically speaking, the envelope of an optical pulse moves at the group velocity while the parameter β_2 represents the different velocity of every spectral component, namely the dispersion of the group velocity and therefore is known as the group-velocity-dispersion (GVD). β_2

is varying with wavelength λ as shown in Figure 1.1 for bulk Silica. One of the most important features of this property is its vanishing at specific wavelength- the zero-dispersion wavelength, denoted as λ_D. At this wavelength the dispersion moves between the two dispersion domains- the normal dispersion regime, in which $\beta_2>0$, and the anomalous dispersion regime in which $\beta_2<0$. In the normal-dispersion regime, high-frequency (blue-shifted) components of an optical pulse travel slower than low-frequency (red-shifted) components of the same pulse. By contrast, the opposite occurs in the anomalous-dispersion regime in which $\beta_2<0$. However, note that dispersion does not vanish at $\lambda=\lambda_D$ because then the third order dispersion (TOD), originating from the cubic term in the Taylor series of $\beta(\omega)$, becomes dominant and cannot be neglected. Such higher-order dispersive effects can distort ultrashort optical pulses both in the linear and nonlinear regimes. The slope of the dispersion curve- $\beta_2(\lambda)$- (called the dispersion slope) is related to the (TOD) parameter β_3.

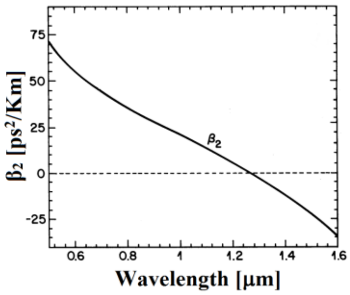

Figure 1.1- Variation of β_2 with wavelength for fused silica. The dispersion parameter $\beta_2=0$ near 1.27μm.

For bulk fused Silica $\lambda_D=1.27\mu m$, but in silica fiber dispersive behavior deviates from that due to small amounts of dopants in the core and due to the waveguide geometry. The main effect of the waveguide contribution is to shift λ_D slightly toward longer wavelengths; λ_D~$1.31\mu m$ for standard fibers and can be shifted further by changing the fabrication process in others (dispersion shifted fibers- DSF).

1.2 Nonlinear phenomena in fibers

The response of any dielectric to light becomes nonlinear for intense electro-magnetic fields, and optical silica fibers are no exception. Nonlinear response means that the total polarization P induced by electric dipoles is not linear in the electric field E, but satisfies the more general relation:

$$P = \varepsilon_0(\chi^{(1)} \cdot E + \chi^{(2)} \cdot EE + \chi^{(3)} \cdot EEE + ...) \qquad \mathbf{1.4}$$

where ε_0 is the vacuum permittivity and $\chi^{(j)}$ (j=1,2…) is the j-th order susceptibility.

The linear susceptibility $\chi^{(1)}$ represents the dominant contribution to P. Its effects are included through the refractive index n and the attenuation coefficient α. The second-order susceptibility $\chi^{(2)}$ is nonzero only for media that lack an inversion symmetry at the atomic or molecular level. As SiO_2 is an amorphous material- what gives it a nature of a symmetric material (from the aspect of the nonlinearity) since it has no orientation, $\chi^{(2)}$ vanishes for silica glasses and as a result, optical fibers do not normally exhibit second-order nonlinear effects.

The lowest-order nonlinear effects in optical fibers originate from the third order susceptibility $\chi^{(3)}$, which is responsible for phenomena such as third harmonic generation, four-wave mixing, and nonlinear refraction, a phenomenon referring to the intensity dependence of the refractive index. In its simplest form, the refractive index can be written as:

$$\tilde{n}(\omega,|E|^2) = n(\omega) + n_2|E|^2 \qquad \textbf{1.5}$$

where $n(\omega)$ is the linear part of the induced polarization, $|E|^2$ is the optical intensity inside the fiber, and n_2 is the nonlinear-index coefficient related to $\chi^{(3)}$ by the relation

$$n_2 = \frac{3}{8n}\mathrm{Re}(\chi^{(3)}_{xxxx}) \qquad \textbf{1.6}$$

where *Re* stands for the real part and the optical field is assumed to be linearly polarized so that only one component $\chi^{(3)}_{xxxx}$ of the fourth-rank tensor contributes to the refractive index.

The intensity dependence of the refractive index leads to a large number of interesting nonlinear effects, two of which are self-phase modulation (SPM) and cross-phase modulation (XPM). Self-phase modulation refers to the self-induced phase shift experienced by an optical field during its propagation in optical fibers. Its magnitude can be obtained by noting that the phase of an optical field changes by

$$\phi = \tilde{n}k_0L = (n + n_2|E|^2)k_0L \qquad \textbf{1.7}$$

where $k_0=2\pi/\lambda$ and L is the fiber length. The intensity-dependent nonlinear phase shift

$$\phi_{NL} = n_2|E|^2 k_0L \qquad \textbf{1.8}$$

is due to SPM. Cross-phase modulation refers to the nonlinear phase shift of an optical field induced by another field having a different wavelength, direction, or state of polarization. This effect is not relevant in our study because we deal with single pulse propagation.

Among other nonlinear effects present in optical fibers are stimulated Raman scattering effects and stimulated Brillouin scattering effects which related to vibrational excitation modes of silica. These effects are encountered when dealing with relatively high power optical fields or very short pulses, as will be detailed in chapter 1.3.

Though the nonlinear coefficient n_2 in bulk fuse silica is ~ 10^{-20} [m^2/W], very small relatively to other nonlinear materials, the nonlinear effects in optical fibers can be observed at relatively low power levels. This is possible because of two important characteristics of single-mode fibers—a small spot size (mode diameter at $\lambda=1.55$ μm~ 10 μm) and extremely low loss (< 1 dB/km) in the wavelength range 1.0–1.6 μm.

1.3 The pulse propagation equation

In this section we introduce the basic equation that governs propagation of optical pulses in nonlinear dispersive fibers in order to understand the interplay between the two phenomena. This equation is useful for the pulse propagation simulations in this work, as will be explained in the chapter "methods".

Starting from the wave equation

$$\nabla^2 E - \frac{1}{c^2}\frac{\partial^2 E}{\partial t^2} = \mu_0 \frac{\partial^2 P_L}{\partial t^2} + \mu_0 \frac{\partial^2 P_{NL}}{\partial t^2} \qquad \textbf{1.9}$$

where the induced polarization P is separated to the linear and nonlinear parts according to the development of the fiber susceptibility into series, as shown in Eq. 2.4, we can derive the pulse propagation equation. Some preliminary assumptions must be taken before the derivation: P_{NL} is treated as a small perturbation to P_L- this is justified because nonlinear changes in the refractive index are < 10^{-6} in practice, and the optical field is assumed to maintain its polarization along the fiber length so that a scalar approach is valid.

The full form of the derived pulse propagation equation is

$$\frac{\partial A}{\partial z} + \frac{\alpha}{2} + \beta_1 \frac{\partial A}{\partial t} + i\frac{\beta_2}{2}\frac{\partial^2 A}{\partial t^2} - \frac{\beta_3}{6}\frac{\partial^3 A}{\partial t^3} = i\gamma(|A|^2 A + \frac{i}{\omega_0}\frac{\partial}{\partial t}(|A|^2 A) - T_R A \frac{\partial |A|^2}{\partial t}) \qquad \textbf{1.10}$$

Where A is the amplitude of the pulse electrical field, α represent the fiber losses, β_1 represent the group velocity of the pulse according the relation $v_g = (\beta_1)^{-1}$, β_2 is the dispersion parameter, β_3 is the TOD parameter, γ is the nonlinear parameter which related to the intensity dependence of the refractive index as detailed in Eq 2.13 and T_R is a parameter related to Raman scattering.

This form includes high orders terms of dispersion and nonlinearity. The equation can be reduced to its simplest form by taking in account some limitations, which enable us to neglect the higher orders terms. First, the optical field is assumed to be quasi-monochromatic, i.e., the pulse spectrum, centered at ω_0, is assumed to have a spectral width $\Delta\omega$ such that $\Delta\omega/\omega_0 \ll 1$. Since $\omega_0 \sim 10^{15} s^{-1}$, the last assumption is valid for pulses as short as 0.1 ps. This assumption is actually slowly varying envelope approximation and therefore the optical field can be written as

$$\boldsymbol{A}(r,t) = \frac{1}{2}\hat{x}[E(r,t)\exp(-i\omega_0 t) + c.c.] \qquad \textbf{1.11}$$

where $\hat{x}$ is the polarization unit vector, and $E(r,t)$ is a slowly varying function of time (relative to the optical period). Considerable additional simplification occurs if the nonlinear response is assumed to be instantaneous. This simplification amounts to neglecting the contribution of molecular vibrations to $\chi^{(3)}$ (the Raman effect) but it is valid only for pulse widths >1 ps. The fiber losses can also be neglected, by assuming the presence of amplifiers along the fiber or by limiting the propagation lengths (before the losses become considerable). Additionally, we choose to "move with the pulse" in its group velocity $v_g = (\beta_1)^{-1}$, such that the time variable t can be replaced by local time variable T which defined as $T = t - \frac{z}{v_g}$ and then the term of the pulse group velocity can be dropped from the pulse propagation equation.

After all the above simplifications are applied and limitations were taken in account, we can neglect the higher orders terms and get the reduced form of the nonlinear pulse propagation equation such that it includes only the second order dispersion and SPM. The reduced equation is now in the form of the Non-Linear Schrödinger Equation (NLSE):

$$\frac{\partial A}{\partial z} + \frac{i\beta_2}{2}\frac{\partial^2 A}{\partial T^2} = i\gamma|A|^2 A \qquad \textbf{1.12}$$

the nonlinear coefficient γ is defined as:

$$\gamma = \frac{n_2\omega_0}{cA_{eff}} \qquad \textbf{1.13}$$

where n_2 is related to the nonlinear response of the fiber and A_{eff} is the effective area of the optical mode in the fiber.

Except for special cases, the NLSE does not have analytical solutions and has to be solved using numerical methods.

In the next sub-sections we will explain how the dispersion and the nonlinear effects influence on the pulse propagation each of them separately and both of them together, according to the NLSE.

1.3.1 Dispersion-induced pulse broadening

In linear media, the pulse propagation is governed by the dispersion equation:

$$i\frac{dU}{dz}=\frac{\beta_2}{2}\frac{d^2U}{dT^2} \qquad \textbf{1.14}$$

where $U(z,T)$ is the normalized amplitude of the pulse such that:

$$U(z,T)=\frac{A(z,T)}{\sqrt{P_0}}, \qquad \textbf{1.15}$$

where P_0 is the peak power.

This equation is obtained by dropping the nonlinear term from the NLSE. The dispersion equation is similar to the paraxial diffraction equation that governs the diffraction of CW light and becomes identical to it when the diffraction occurs in only one transverse direction and β_2 is replaced by $\lambda/2\pi$, where λ is the wavelength of light. For this reason, the dispersion-induced temporal effects have a close analogy with the diffraction-induced spatial effects, except for the fact that the dispersion can be negative or positive but diffraction is one sided (unless negative index material is considered).

Using the Fourier-transform method, we get the Fourier transform of the solution of the dispersion equation:

$$\tilde{U}(z,\omega)=\tilde{U}(0,\omega)\exp(\frac{1}{2}\beta_2\omega^2 z)\,. \qquad \textbf{1.16}$$

This solution shows that GVD changes the phase of each spectral component of the pulse by an amount that depends on both the frequency and the propagated distance. Even though such phase changes do not affect the pulse power spectrum, they can modify the pulse shape.

As a simple example, consider the case of a Gaussian pulse for which the incident field is of the form

$$U(0,T) = \exp(-\frac{T^2}{2T_0^2}) \quad \textbf{1.17}$$

where T_0 is the half-width (at 1/e-intensity point). After obtaining $\tilde{U}(0,\omega)$, substituting it in the Fourier solution and converting back to time, we get:

$$U(z,T) = \frac{T_0}{\sqrt{T_0^2 - i\beta_2 z}} \exp\left(-\frac{T^2}{2(T_0^2 - i\beta_2 z)}\right).$$

Thus, a Gaussian pulse maintains its shape on propagation but its width T_1 increases with z as $T_1(z) = T_0\sqrt{1+(z/L_d)^2}$ where L_D, the characteristic length of the dispersion, is defined as:

$$L_D = \frac{T_0^2}{|\beta_2|}. \quad \textbf{1.18}$$

According to this definition, at $z=L_D$, a Gaussian pulse broadens by a factor of $\sqrt{2}$. For a given fiber length, short pulses broaden more because of a smaller dispersion length. The broadening of a Gaussian pulse is shown in Figure 1.2 (a). In Figure 1.2(b) we can see the pulse power spectrum which remains unchanged throughout propagation.

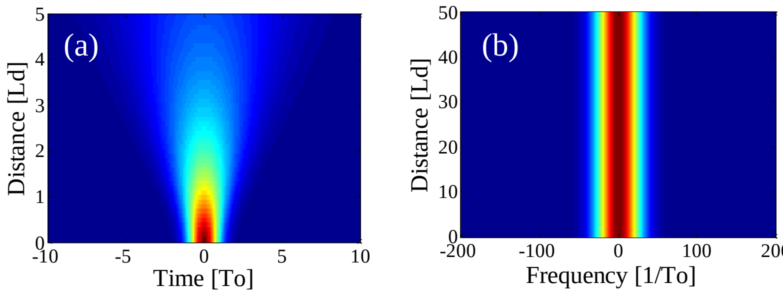

Figure 1.2- Propagation images of initially unchirped Gaussian pulse under the influence of chromatic dispersion (a)in the time domain and (b) in the frequency domain.

This broadening is caused by induced chirping during the pulse propagation. The chirping can be seen clearly by writing $U(z,T)$ in the form $U(z,T) = |U(z,T)|\exp(i\phi(z,T))$ such that:

$$\phi(z,T) = \frac{\operatorname{sgn}(\beta_2)(z/L_D)}{1+(z/L_D)^2}\frac{T^2}{T_0^2} + \frac{1}{2}\tan^{-1}(\frac{z}{L_d}) \quad \textbf{1.19}$$

The time dependence of the phase $\varphi(z,T)$ implies that the instantaneous frequency differs across the pulse from the central frequency ω_0. The difference $\delta\omega$ is just the time derivative $\partial\phi/\partial T$ and is given by

$$\delta\omega(T) = \frac{d\phi(z,T)}{dT} = \frac{\mathrm{sgn}(\beta_2)(2z/L_D)}{1+(z/L_D)^2}\frac{T}{T_0^2}. \qquad \textbf{1.20}$$

This derivative shows that the frequency changes linearly across the pulse, i.e., a fiber imposes linear frequency chirp on the pulse. The chirp $\delta\omega$ depends on the sign of β_2. In the normal-dispersion regime ($\beta_2>0$), $\delta\omega$ is negative at the leading edge ($T<0$) and increases linearly across the pulse; the opposite occurs in the anomalous-dispersion regime ($\beta_2>0$). This relations between the frequency and the time causes different frequency components of a pulse to travel at slightly different speeds along the fiber and hence to arrive to its end at different times. The pulse can maintain its width only if all spectral components arrive together. Any time delay in the arrival of different spectral components leads to pulse broadening.

1.3.2 SPM-Induced Spectral Broadening

When the pulse width is wide enough while its peak power is high, we can neglect the dispersion term from the NLSE and get the equation which governs the pulse propagation under the influence of SPM only:

$$\frac{\partial U}{\partial z} = \frac{i}{L_{NL}}|U|^2 U \qquad \textbf{1.21}$$

where U is the normalized amplitude $U(z,T)$ of the pulse, as defined in Eq. 2.15 and L_{NL} is the nonlinear length defined as

$$L_{NL} = (\gamma P_0)^{-1}. \qquad \textbf{1.22}$$

The equation can be solved substituting $U=V\exp(i\phi_{NL})$ and equating the real and imaginary parts so that

$$\frac{\partial V}{\partial z} = 0; \quad \frac{\partial \varphi_{NL}}{\partial z} = \frac{1}{L_{NL}}|V|^2 \qquad \textbf{1.23}$$

The general solution of $U(L,T)$ is

$$U(L,T) = U(0,T)\exp[i\phi_{NL}(L,T)] \qquad \textbf{1.24}$$

where

$$\phi_{NL}(L,T) = |U(0,T)|^2 \frac{L}{L_{NL}}. \qquad \textbf{1.25}$$

These solutions show that SPM gives rise to an intensity-dependent phase shift but the pulse shape remains unaffected, as seen in Figure 1.3(a). The nonlinear phase shift ϕ_{NL} increases with fiber length L but the maximum phase shift φ_{max} occurs at the pulse peak center located at $T=0$. With U normalized such that $|U(0,0)|=1$, it is given by

$$\varphi_{\max} = |U(0,T)|^2 \frac{L}{L_{NL}} = \gamma P_0 L. \qquad \textbf{1.26}$$

The physical meaning of the nonlinear length L_{NL} is clear from this expression—it is the effective propagation distance at which ϕ_{max} =1.

The SPM-induced spectral broadening is a consequence of the time dependence of ϕ_{NL}. This can be understood by noting that a temporally varying phase implies that the instantaneous optical frequency differs across the pulse from its central value ω_0. The difference $\delta\omega$ is given by

$$\delta\omega(T) = -\frac{\partial \phi_{NL}}{\partial T} = -\frac{L}{L_{NL}} \frac{\partial}{\partial T} |U(0,T)|^2 \qquad \textbf{1.27}$$

where the minus sign is due to the choice of the factor $exp(-i\omega_0 t)$ in the propagated field definition. The time dependence of $\delta\omega$ is referred to as frequency chirping and the chirp induced by SPM increases in magnitude with the propagated distance. In other words, new frequency components are generated continuously as the pulse propagates down the fiber. These SPM-generated frequency components broaden the spectrum over its initial width at $z=0$, depending on the pulse shape but they don't walk off since there is no dispersion. Consider, for example, the case of Gaussian pulse with the incident field $U(0,T)=exp[-(T/T_0)^2]$. The SPM-induced chirp $\delta\omega(T)$ for such a pulse is

$$\delta\omega(T) = \frac{L}{L_{NL}} \frac{4T}{T_0^2} \exp\left[-2\left(\frac{T}{T_0}\right)^2\right]. \qquad \textbf{1.28}$$

The temporal variation of the induced chirp $\delta\omega$ has several interesting features. First, $\delta\omega$ is negative near the leading edge, when $T<0$ (red shift) and becomes positive near the trailing edge, when $T>0$ (blue shift) of the pulse. Second, the chirp is linear and positive (up-chirp) over a large central region of the Gaussian pulse. Third, the chirp is considerably larger for pulses with steeper leading and trailing edges.

An estimate of the magnitude of SPM-induced spectral broadening can be obtained by calculating the peak value of $\delta\omega(T)$. By setting its time derivative to zero, the maximum value of $\delta\omega$ (for Gaussian pulse) is related to ϕ_{max} and given by

$$\delta\omega_{\max} = 0.86 \Delta\omega_0 \phi_{\max} \qquad \textbf{1.29}$$

where $\Delta\omega_0 = T_0^{-1}$ is the initial spectral width of the pulse.

In the case of intense ultrashort pulses, the broadened spectrum can extend over 100 THz or more, especially when SPM is accompanied by other nonlinear processes such as stimulated Raman scattering and four-wave mixing. Such an extreme spectral broadening is referred to as supercontinuum.

The actual shape of the pulse power spectrum *S(ω)*, as seen in Figure 1.3(b), is obtained by taking the Fourier transform of *U(L,T)*, using the relation $S(\omega) = \left|\tilde{U}(L,\omega)\right|^2$. The most notable feature of the pulse spectrum shape is that SPM-induced spectral broadening have an oscillatory structure covering the entire frequency range. In general, the spectrum consists of many peaks, and the outermost peaks are the most intense. The number of peaks depends on ϕ_{max} and increases linearly with it. The origin of the oscillatory structure can be understood by the time dependence of the SPM-induced frequency chirp. In general, the same chirp occurs at two values of *T* showing that the pulse has the same instantaneous frequency at two distinct points. Qualitatively speaking, these two points represent two waves of the same frequency but different phases that can interfere constructively or destructively depending on their relative phase difference. Mathematically, the Fourier integral in *S(ω)* calculation gets dominant contributions at the two values of *T* at which the chirp is the same. These contributions, being complex quantities, may add up in phase or out of phase.

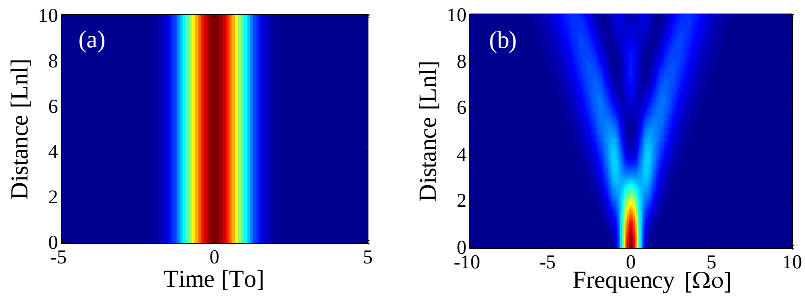

Figure 1.3- Propagation image of Gaussian pulse under the influence of SPM (a) in the time domain and (b) in the frequency domain.

The number of peaks M in the SPM-broadened spectrum is given approximately by the relation $\phi_{max} \approx (M-1/2)\pi$.

For pulses with steeper leading and trailing edges (such as rectangular pulse) the spectral width after SPM broadening is extend over a longer frequency range than pulses with moderate edges slope (such as Gaussian) with the same initial width and propagation distance, but the tails of the steeper pulses spectrum carry less energy because the chirping occurs over a small time duration.

1.3.3 Effect of Group-Velocity Dispersion with Self-Phase Modulation

As pulses become shorter and the dispersion length becomes comparable to the fiber length, it becomes necessary to consider the combined effects of GVD and SPM. This section considers the temporal and spectral changes that occur when the effects of GVD are included in the description of SPM.

The starting point in the analyzing of the combined effect is the nonlinear Schrodinger (NLS) equation which can be written in a normalized form as

$$i\frac{\partial U}{\partial \xi} = \mathrm{sgn}(\beta_2)\frac{1}{2}\frac{\partial^2 U}{\partial \tau^2} - N^2|U|^2 U \qquad \mathbf{1.30}$$

where ξ and τ represent the normalized distance and time variables defined as

$$\xi = \frac{z}{L_d}; \quad \tau = \frac{T}{T_0} \qquad \mathbf{1.31}$$

and the parameter N is defined as:

$$N^2 = \frac{L_d}{L_{NL}} = \frac{\gamma P_0 T_0^2}{|\beta_2|}. \qquad \mathbf{1.32}$$

As evident from this relation, N governs the relative importance of the SPM and GVD effects on pulse evolution along the fiber. Dispersion dominates for $N<1$ while SPM dominates for $N>1$. For values of $N\sim 1$, both SPM and GVD play an equally important role during pulse evolution. In the NLSE, $sgn(\beta_2)=\pm 1$ depending on whether GVD is normal ($\beta_2>0$) or anomalous ($\beta_2<0$). The physical significance of N will become clear in Chapter 1.5- The soliton pulse, where the integer values of N are found to be related to the soliton order.

When $N=1$, the evolution of the shape and the spectrum of an initially unchirped Gaussian pulse in the normal-dispersion regime (Figure 1.4(a)) of a fiber is quite different from that expected when either GVD or SPM dominates. In particular, the pulse broadens much more rapidly compared with the $N=0$ case (no SPM). This can be understood by noting that SPM generates new frequency components that are red-shifted near the leading edge and blue-shifted near the trailing edge of the pulse. As the red components travel faster than the blue components in the normal-dispersion regime, SPM leads to an enhanced rate of pulse broadening compared with that expected from GVD alone. This in turn affects spectral broadening as the SPM-induced phase shift ϕ_{NL} becomes less than that occurring if the pulse shape were to remain unchanged.

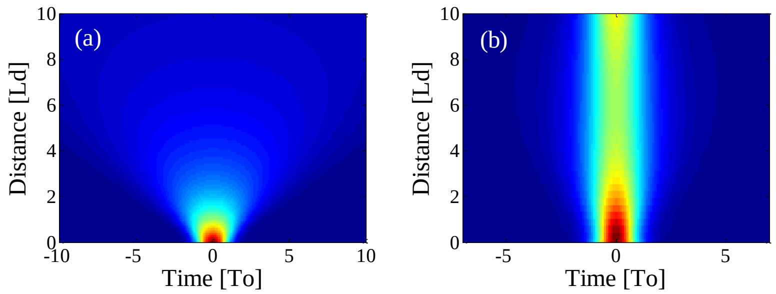

Figure 1.4- Propagation image of initially unchirped Gaussian pulse for N=1 at (a) normal dispersion and (b) anomalous dispersion.

The situation is different for pulses propagating in the anomalous-dispersion regime of the fiber, when N is still ~1, but the sign of the GVD parameter has been reversed ($\beta_2<0$). As can be seen in Figure 1.4(b), the pulse broadens initially at a rate much lower than that expected in the absence of SPM and then appears to reach a steady state. At the same time, the spectrum narrows rather than exhibiting broadening expected by SPM in the absence of GVD. This behavior can be understood by noting that the SPM-induced chirp is positive while the dispersion-induced chirp for anomalous dispersion ($\beta_2<0$) is negative. The two chirp contributions nearly cancel each other along the center portion of the Gaussian pulse when $L_D=L_{NL}$ ($N=1$). Pulse shape adjusts itself during propagation to make such cancelation as complete as possible. Thus, GVD and SPM cooperate with each other to maintain a chirp-free pulse. The preceding scenario corresponds to soliton evolution; initial broadening of the Gaussian pulse occurs because the Gaussian profile is not the characteristic shape associated with a fundamental soliton. Indeed, if the input pulse is chosen to be a "sech" pulse both its shape and spectrum remain unchanged during propagation. When the input pulse deviates from a 'sech' shape, the combination of GVD and SPM affects the pulse in such a way that it evolves to become a 'sech' pulse. This aspect is discussed in detail in Chapter 1.5 and along this work.

When $N \gg 1$ the effects of SPM should dominate over those of GVD for, at least, the initial stages of pulse evolution. It is true only for the first stage because when a large amount of the SPM-induced frequency chirp imposed on the pulse, even weak dispersive effects lead to significant pulse shaping. In the case of normal dispersion ($\beta_2>0$), the pulse becomes nearly rectangular with relatively sharp leading and trailing edges and is accompanied by a linear chirp across its entire width. It is this linear chirp that can be used to compress the pulse by passing it through a dispersive delay line.

1.4 The Airy pulse

Nondiffracting beams are beams that have special functional form such that they can propagate in diffractive medium without reshaping. A well-known class of nondiffracting beams is Bessel beams [2]. The functional form of these beams is defined by Bessel functions, which are a solution of the wave equation. These beams have cylindrical symmetry, constructed from one circular spot and infinite rings around it. Practically, Bessel beams cannot have infinite amount of rings because it requires infinite amount of energy. Thus, practical implementations introduce apodization, causing the Bessel beam to finally diffracted, but it remains unchanged for considerable long distance- relative to the regular Gaussian beams. Bessel beams were found to be useful and efficient in optical tweezers (controlling on particles and cells movement by light) due to their continuous focus caused by the nondifracting feature. Similar nondiffracting beam class is the Airy beams.

The Airy function *Ai(s)* is one sided, oscillating function also having infinite energy. This function was originally [3] proposed in the context of quantum mechanics as a nonspreading solution to the Schrödinger equation for free particles. Later, it was demonstrated [4] that this function is also solution of the paraxial diffraction equation

$$i\frac{\partial A}{\partial \xi}+\frac{1}{2}\frac{\partial^2 A}{\partial s^2}=0 \qquad \textbf{1.33}$$

(where A is normalized optical field amplitude, ξ represent the normalized propagation distance and s represents a dimensionless spatial transverse coordinate),
and therefore it can describe an optical beam. This optical beam found to have two unique interesting features: self-similarity where during propagation the wavefront maintains its shape in the presence of diffraction—the nondiffracting feature being similarly to the Bessel beams—and ballistic dynamics where its wavefront travels along a parabolic trajectory without the presence of any external potential.

The propagation of temporal pulses in linear media is described by the dispersion equation

$$i\frac{\partial A}{\partial z}=\frac{\beta_2}{2}\frac{\partial^2 A}{\partial T^2} \quad \textbf{1.34}$$

where A is normalized optical field amplitude, z represent the propagation distance, T represents a time variable in frame of reference that moves in the group velocity and β_2 is the dispersion coefficient. The isomorphism between the dispersion equation and the paraxial diffraction equation shows that Airy pulses, whose electric field temporal profile is defined by an Airy function, also have the two unique features of self-similarity along the propagation despite the dispersion and acceleration of the Airy wavefront in a time frame moving at the group velocity, as seen at Figure 1.5.

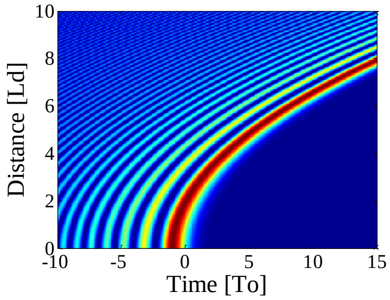

Figure 1.5- Propagation image of ideal Airy pulse. The pulse maintains its intensity distribution and moves along parabolic trajectory.

However, true Airy pulses are impractical as they contain an infinite amount of energy, as with the Bessel beams. By apodizing the Airy pulse, i.e. truncating the semi-infinite oscillations, in our case with a decaying exponential envelope as shown in Figure 1.6(a), the waveform maintains its two unique properties over an extended propagation range despite its finite energy (Figure 1.6(b)).

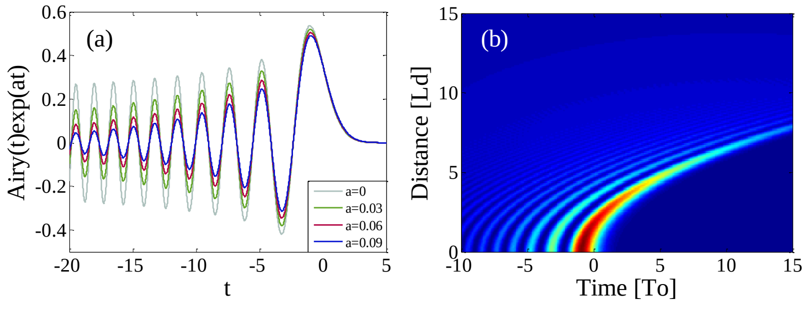

Figure 1.6- (a) Truncated Airy initial profiles for select truncation values. (b) Propagation image of truncated Airy when a=0.05.

According to the Ehrenfest's theorem, the center of mass of every wave packet must remain unchanged when there is no external force, as in our system. Airy pulses and beams appear to violate this rule, but in fact do not as the center of mass of the Airy wave packet cannot be defined and therefore do not conflict with Ehrenfest's theorem. In the case of finite energy-Airy-packet, the center of mass is well defined and in fact remains invariant with distance, what forces the intensity of the accelerating peak to decrease throughout propagation.

In the case of linear propagation, the launched field described by

$$U(s,0) = \mathrm{Airy}(s)\exp(as), \qquad \textbf{1.35}$$

where the truncation degree is determined by the truncation coefficient $0<a<1$ in the decaying exponential envelope $exp(as)$. As a is smaller, the truncation is weaker and the Airy pulse maintains its unique properties for longer propagation distances.

The analytical description of the truncated Airy at any point in its propagation is [4]:

$$U(s,\xi) = \mathrm{Airy}\left[s-(\xi/2)^2 + ia\xi\right]\exp\left[as-(a\xi^2/2)-i(\xi^3/12)+i(a^2\xi/2)+i(\xi s/2)\right]. \qquad \textbf{1.36}$$

From the argument of the Airy function one can conclude that this beam follows a ballistic trajectory in the s–ξ plane that is described by the parabola $s=\xi^2/2$.

In order to move from spatial Airy to temporal Airy we replace the spatial transverse coordinate s by T/T_0, and the normalized distance variable ξ by z/L_D.

The Fourier spectrum of the initial truncated Airy pulse in the normalized ω-space is given by

$$\varphi(\omega,0) = \exp(-a\omega^2)\exp\left(\frac{i}{3}(\omega^3 - 3a^2\omega - ia^3)\right). \qquad \textbf{1.37}$$

According to this expression, it is clear that truncated Airy pulses occur naturally if a Gaussian pulse is propagated in a fiber at the zero dispersion point, under the influence of cubic dispersion, which gives to the Gaussian spectrum a cubic phase and then it translates to Airy distribution in the time domain.

Spatial Airy beams have been investigated extensively in the last few years, and found to be useful for various applications such as: optical micromanipulation when the ballistic dynamics is exploited for process of optically mediated particles clearing[5], optical switching by changing the accelerating direction of the Airy beam in the nonlinear crystal in which it generated [6], the first curved plasma channels generation in air [7] and in water [8] using femtosecond Airy beams[7], what can lead to novel applications in remote sensing, terahertz generation and lightning control . More recently, temporal Airy pulses are being investigated, in the context of spatiotemporal light bullets in linear conditions, where the configuration of Airy-Bessel temporal beam contributes to the versatility of the bullet [9] and in nonlinear conditions- where the three dimensional Airy found to be robust up to the high intensity [10], and in the context of one dimensional Airy pulse propagation, under the influence of strong nonlinearity giving rise to supercontinuum and solitary wave generation [11].

1.5 The soliton pulse

A fascinating manifestation of the fiber nonlinearity occurs through optical solitons [12], formed as a result of the interplay between the dispersive and nonlinear effects. The word soliton refers to special kinds of wave packets that can propagate undistorted over distance. Solitons have been discovered in many branches of physics. In the context of optical fibers, not only are solitons of fundamental interest but they have also found practical applications in the field of fiber-optic communications. This section is devoted to the study of pulse propagation in optical fibers in the regime in which both the group-velocity dispersion (GVD) and self-phase modulation (SPM) are equally important and must be considered simultaneously.

The soliton is a solution of the NLSE and is obtained using the inverse scattering method. Although the NLSE supports solitons for both normal and anomalous GVD, pulse-like solitons- also called bright solitons- are found only in the case of anomalous dispersion. In the case of normal dispersion ($\beta_2>0$), the solutions exhibit a dip in a constant-intensity background. Such solutions are referred to as dark solitons.

Starting from the normalized form of the NLSE when $\beta_2<0$

$$i\frac{\partial U}{\partial \xi}=-\frac{1}{2}\frac{\partial^2 U}{\partial \tau^2}-N^2\left|U\right|^2 U, \qquad \textbf{1.38}$$

where ξ and τ represent the normalized distance and time variables defined as

$$\xi=\frac{z}{L_d},\tau=\frac{T}{T_0} \qquad \textbf{1.39}$$

and the parameter N, which determine the order of the solution, is introduced by

$$N^2=\frac{L_d}{L_{NL}}=\frac{\gamma P_0 T_0^2}{\beta_2}, \qquad \textbf{1.40}$$

one can get the complex eigenvalues of the problem. The number of the eigenvalues is in accordance with the integer N, and they are determining the properties of the solution, such as its group velocity- frequency shift from the carrier frequency, its amplitude(s), its time position and its initial phase. Due to the ability of choosing the axes system and the carrier frequency as we need, in the case of single soliton the most relevant property is the amplitude of the soliton such that the fundamental solitons then form a single-parameter family described by

$$U(\xi,\tau) = A\operatorname{sech}(A\tau)\exp(iA^2 \xi/2). \qquad \mathbf{1.41}$$

The parameter A determines not only the soliton amplitude but also its width. In real units, the soliton width changes with A as T_0/A, i.e., it scales inversely with the soliton amplitude. This inverse relationship between the amplitude and the width of a soliton is the most crucial property of solitons.

In the context of optical fibers, the solution indicates that if a hyperbolic-secant pulse, whose width T_0 and the peak power P_0 are chosen such that $N=1$ is launched inside an ideal lossless fiber, the pulse will propagate undistorted without change in shape for arbitrarily long distance because the propagation distance affects only the accumulated phase, not the pulse intensity, as shown in Figure 1.7(a). It is this feature of the fundamental solitons that makes them attractive for optical communication systems.

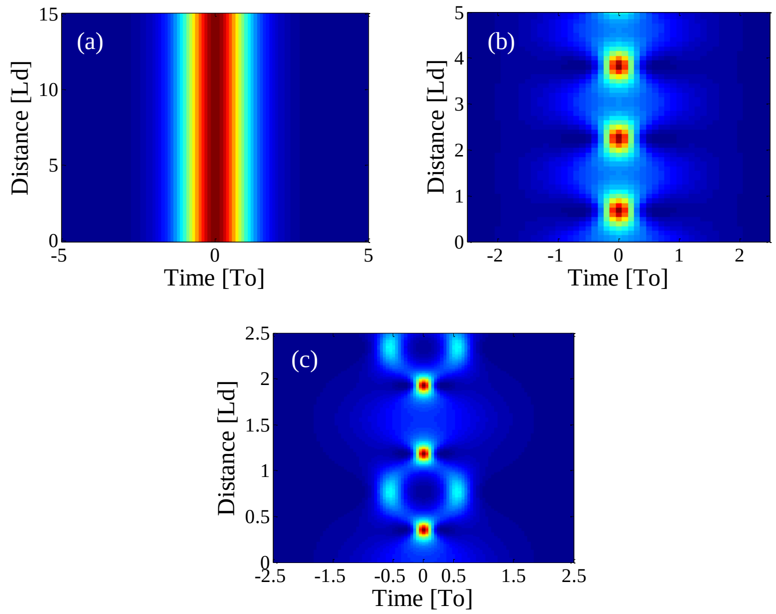

Figure 1.7- Propagation image of (a) first order soliton, (b) second order soliton and (c) third order soliton. It is easy to see that the periodicity of the higher order soliton.

Pulses corresponding to other integer values of N are called higher-order solitons and they do not maintain the initial shape but follow a periodic pattern such that the input shape is recovered at $\xi=m\pi/2$, where m is an integer. The periodic evolution is a result of the imbalance between the dispersion and SPM when $N>1$. SPM dominates initially but GVD soon catches up and leads to pulse contraction and the two effects can cooperate in such a way that the pulse follows a periodic evolution pattern with original shape recurring at multiples of fixed distances. This periodicity is shown in Figure 1.7(b-c), at the propagation image of 2^{rd} and 3^{rd} soliton orders. By noting that $\xi = z/L_D$, the soliton period z_0, defined as the distance over which higher-order solitons recover their original shape, is given by

$$z_0 = \frac{\pi}{2} L_d = \frac{\pi}{2} \frac{T_0^2}{\beta_2}. \tag{1.42}$$

This parameter plays an important role in the theory of optical solitons.

Soliton stability

An important property of optical solitons is that they are remarkably stable against perturbations. Thus, even though the fundamental soliton requires a specific shape and a certain peak power corresponding to $N=1$, it can be created even when the pulse shape and the peak power deviate from the ideal conditions. For example, in the evolution of a Gaussian input pulse for which $N=1$ but $u(0,\tau)=exp(-\tau^2/2)$, the pulse adjusts its shape and width in an attempt to become a fundamental soliton and attains a "sech" profile for $\xi \gg 1$. A similar behavior is observed when N deviates from 1. It turns out that the Nth-order soliton can be formed when the input value of N is in the range $N-1/2$ to $N+1/2$. Due to the fact that the soliton area (normalized by the product of peak power and duration) is equal to $N\pi$, this rule actually stems from to the soliton area theorem [13] which claims that first order soliton can be formed when the area of the input pulse is in the range π/2-3π/2, as long as its shape is similar to that of soliton.

A simple way to understand this behavior [12] is to think of optical solitons as the temporal modes of a nonlinear waveguide. Higher intensities in the pulse center create a temporal waveguide by increasing the refractive index only in the central part of the pulse. Such a waveguide supports temporal modes just as the core-cladding index difference leads to spatial modes. When an input pulse does not match a temporal mode precisely but is close to it, most of the pulse energy can still be coupled into that temporal mode. The rest of the energy spreads in the form of dispersive waves, known as the continuum radiation. It will be seen later that such dispersive waves affect the system performance and should be minimized by matching the input conditions as close to the ideal requirements as possible. When solitons adapt to perturbations adiabatically, perturbation theory developed specifically for solitons can be used to study how the soliton fundamental parameters of amplitude, width, frequency, speed, and phase evolve along the fiber.

2 Goals

In this study, we intend to analyze intense temporal Airy pulse propagation in media exhibiting Kerr nonlinearity as occurring in single mode silica fibers, leading to the phenomena of self-phase modulation (SPM) and anomalous dispersion. The unique features of the Airy pulse are determined by the dispersion equation, which refer only to linear media [3][4]. When the intensity of the Airy pulse is increased the nonlinear response of the media start to influence and must be considered such that the known evolution of the Airy pulse is no longer valid. We want to investigate the deviations of the Airy pulse nonlinear evolution from its linear evolution as the pulse intensity is increased gradually. The influence of the Kerr nonlinear effect on spatial Airy beams has been already investigated under relatively weak parameters and transient narrowing of the Airy main lobe—caused by self-focusing (this is nonlinear effect which is analog to the SPM in temporal pulses)—was observed [14]; however, we are interested in operating under much higher intensities where the nonlinear effect results in soliton shedding from the Airy pulse, according to soliton theory as was detailed in the previous chapter, and not just a small perturbation of the Airy pulse.

Additional investigated aspect of the nonlinear Airy pulse propagation is the truncation degree influence. By comparison to its influence on the propagation in the linear regime we shall study the truncation role in the Airy pulse nonlinear evolution.

Although we analyze temporal Airy pulse propagation in fiber, our results are also valid for spatial Airy beams diffracting in Kerr media on account of the isomorphism between the dispersion equation and the paraxial diffraction equation.

3 Methods- Numerical Simulation for pulse propagation

In this study we simulated the propagation of Airy pulse in nonlinear media. As mentioned before, the propagation is governed by the NLSE which cannot be solved analytically except for special cases and therefore it must be solved numerically.

Many numerical methods can be employed in order to simulate the pulse propagation [1]. These can be classified into two broad categories known as: (i) the finite-difference methods, in which a is solved by approximating the derivatives by finite differences that can be calculated numerically; and (ii) pseudospectral methods, in which the derivatives in partial differential equation are calculated using orthogonal functions, e.g Fourier integrals. In general, pseudospectral methods are faster by up to an order of magnitude to achieve the same accuracy due to the use of the finite-Fourier-transform (FFT) algorithm.

We use the Split Step Fourier Method (SSFM), which belongs to the last category for its simplicity, flexibility and efficiency.

3.1 Introduction to the Split Step Fourier method

The NLSE can be written in the operator form

$$\frac{\partial A}{\partial z} = (\hat{D} + \hat{N})A \qquad \textbf{3.1}$$

where A is the optical field amplitude, $\hat{D}$ is a differential operator that accounts for dispersion in a linear medium and $\hat{N}$ is a nonlinear operator that governs the effect of fiber nonlinearities on pulse propagation. These operators are given by

$$\hat{D} = -\frac{i\beta_2}{2}\frac{\partial^2}{\partial T^2}, \qquad \textbf{3.2}$$

$$\hat{N} = -i\gamma|A|^2. \qquad \textbf{3.3}$$

In general, dispersion and nonlinearity act together along the length of the fiber. The split-step Fourier method obtains an approximate solution by assuming that in propagating the optical field over a small distance h, the dispersive and nonlinear effects can be assumed to act independently. More specifically, propagation from z to

$z+h$ is carried out in two steps. In the first step, the nonlinearity acts alone, and $\hat{D}=0$. In the second step, dispersion acts alone, and $\hat{N}=0$. Mathematically:

$$A(z+h,T) \approx \exp(h\hat{D})\exp(h\hat{N})A(z,T) \qquad \mathbf{3.4}$$

The dispersion step has an analytical solution in the frequency domain where $\hat{D}$ can be replaced by $\frac{i\beta_2}{2}(\omega-\omega_0)^2$-where ω_0 is the carrier frequency, so it is necessary to Fourier transform *A(z,T)* before applying this step, using

$$\tilde{A}(z,\omega)=\int_{-\infty}^{\infty} A(z,T)\exp(i(\omega-\omega_0))dT, \qquad \mathbf{3.5}$$

and then applying the dispersion operator such that

$$\tilde{A}(z+h,\omega)=\exp(i\frac{\beta_2}{2}(\omega-\omega_0)^2 h)\tilde{A}(z,\omega). \qquad \mathbf{3.6}$$

The nonlinear step is done in the time domain so it is required to do inverse Fourier transform after applying the dispersion step.

When the fiber length is divided into a large number of segments in length *h*, the optical pulse is propagated from segment to segment by applying the mentioned above dispersion and nonlinear operators and we get good approximation of the pulse propagation along the fiber length. All the transitions between the time domain and the frequency domain are computed by the FFT algorithm that makes numerical evaluation of the propagation equation relatively fast.

In this work we used an improved form of the basic SSFM by dividing every segment to two parts and apply the dispersion operator on the first half of the segment, then operate on a full segment with the nonlinear operator and complete the segment with applying of the dispersion operator for the remaining half segment. The advantage gained through this variation is that the nonlinear contribution is not taken at the boundaries but at the middle of the segment, averaging out of the nonlinear property.

3.2 The algorithm

Our algorithm is developed based on the last variation (the Matlab simulation code is given in appendix A):

- Step 1: Divide the fiber into segments (Figure 3.1).
- Step 2: Split the segment in two equal parts.
- Step 3: Operate on the first half with the dispersion operator.

- Step 4: Operate on the entire segment with the nonlinear operator.
- Step 5: Operate on the second half with the dispersion operator.
- Step 6: Repeat steps two through five for the adjacent segment with the result obtained from the previous segments.

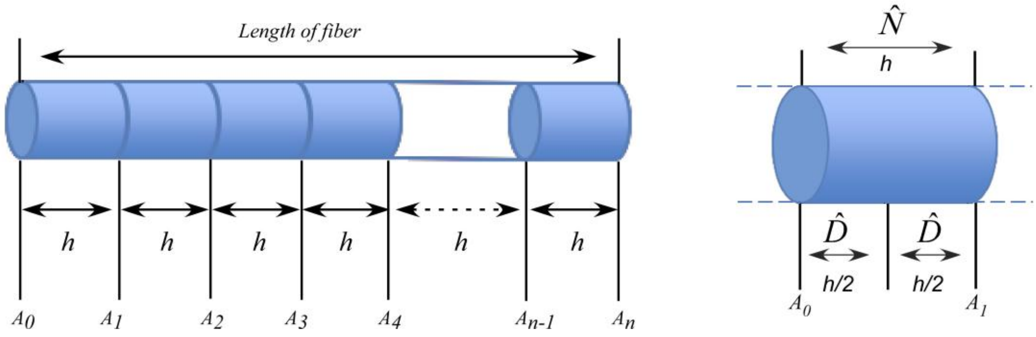

Figure 3.1- Segmentation of the fiber into parts at length h and further separation of a single segment into two parts in order to improve the accuracy

3.3 Consideration and limitations

There are some considerations that must be addressed prior to the application of SSFM. The prominent one is the step size h (the length of a fiber segment).

In order to acquire reasonable accuracy we aspire that h be a least two orders of magnitude less than the characteristic length of the dominant phenomena governing the propagation. However, this length is not necessarily constant, and the optimum choice h depends on the complexity of the problem at hand. For example, during propagation self-focusing of the Airy main lobe will increase its peak power, resulting in a decrease in L_{NL}, and h must be reduced as well, as changes will now occur at a faster pace. Therefore, in order to take into account such scenarios, we take h to be at least three orders of magnitude smaller than the initial dominate characteristic length. We compared the analytical propagation of first order soliton with its numerical propagation under such conditions of increment size and we found that they are identical up to 10 orders of magnitude. These results demonstrate that the algorithm is accurate and reliable for our simulation.

Additional property that must be considered is range of the transverse coordinate- the time window in our case. Due to the circular assumption behind the Fast Fourier transform, when pulse energy reaches the ends of the time window it will continue and re-imerge from the other end, creating unphysical results. This can be overcome by simply making the time window large enough. This solution requires large vectors resulting in more processing time and more memory. A more advance solution is to multiply the optical field at every step by rectangular-like function- "absorbing edge"- and this way to "cut off" the spreading energy and preventing the feedback. The rectangular-like function must be chosen such that a gradual cutoff of the edge will be carried out because an abrupt cutoff can generate a reflection. The main disadvantage of using the absorbing edge is that it does not preserve the pulse energy when the pulse reaches the edge.

In our work (see Figure 3.2), we use time vector whose range is more than thousand times the width of the Airy main lobe and its resolution is tenth of its width. This large time window is required due to the ballistic dynamics of the Airy pulse which cause rapid energy spreading, especially for small truncation values, when the carried energy is almost infinite. In addition, we used an absorbing edge of the form "raised-cosine" function, in which the rectangular-like degree is defined by $0<\beta<1$. We fixed this parameter on 0.01, causing its corner to be relatively sharp, in order to prevent loss of the pulse energy. Despite the sharpness of the absorbing edge, any energy reflection from the window boundaries is not observed thanks to the large time window.

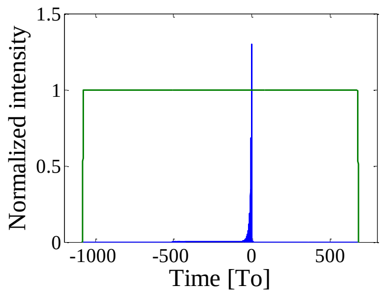

Figure 3.2- Launched Airy pulse (blue) compared to the raised-cosine absorbing edge (green)

Normalization terms

In our simulations we used the normalized NLSE form

$$i\frac{\partial A}{\partial z}=\mathrm{sgn}(\beta_2)\frac{1}{2}\frac{\partial^2 A}{\partial T^2}-|A|^2 A, \qquad \textbf{3.7}$$

where $|\beta_2|=\gamma=T_0=1$, and the launched Airy pulse profile is defined as:

$$A(T,z=0)=\sqrt{R\cdot K_p(a)}\cdot Ai(T)\cdot Exp(a\cdot T) \qquad \textbf{3.8}$$

where $0<a<1$ is the truncation coefficient, and $K_p(a)$ is a truncation-dependent factor that sets the pulse peak intensity to 1 for any a value . This factor was numerically calculated and found to be in parabolic dependence with the truncation coefficient. T is the time variable in a frame of reference that moves with the wave group velocity, i.e. $T = t - z/v_g$, and R is a dimensionless parameter we vary for scaling the Airy power. At $R=1$ the Airy main lobe intensity profile looks quite similar to the fundamental soliton, as shown in Figure 3.3.

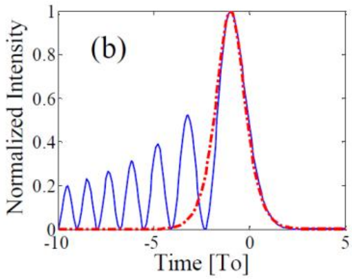

Figure 3.3 – Launched Airy pulse in time (blue solid curve), compared to a soliton pulse (red dashed curve).

We measure the propagation distance in L_d units, defined as $L_d = T_0^{\,2}/\beta_2$, which in our normalized coordinates equals 1.

It is important to note that even though we use dimensionless parameters in our simulation they are reliable only for propagation of pulses whose width is wider than 5 ps. When dealing with pulses that are less than 5ps, further terms must be taken into account in the pulse propagation equation, as detailed in the extended pulse propagation equation, in order to include additional nonlinear phenomena.

4 Airy propagation in nonlinear media- simulations result and analysis

4.1 Effects of launched Airy power

In order to investigate the influence of Airy launched power on its evolution, we varied the scaling parameter R from the equation

$$A(z=0,T) = R \cdot K_p(a) \cdot Ai(T)\exp(T) \qquad \mathbf{4.1}$$

in the range 0.1-2 and for every R value we propagate the pulse using the SSFM algorithm. Figure 4.1 shows pulse evolution examples for select R values. At low launched power, the Airy pulse performs the acceleration in time and subsequently it succumbs to dispersion. However, when R is sufficiently large (above 0.9) a stationary soliton pulse is formed out of the centered energy about the Airy main lobe. The soliton exhibits periodic oscillations in the soliton amplitude and width as a function of propagation distance. In addition, we witness the resilience of the temporal Airy waveform to shedding of a fraction of the energy as a soliton; the wavefront continues to propagate along a parabolic trajectory. Similar resilience has been shown in main lobe masking for spatial Airy beams [15] and in supercontinuum generation for temporal Airy pulses propagation[11].

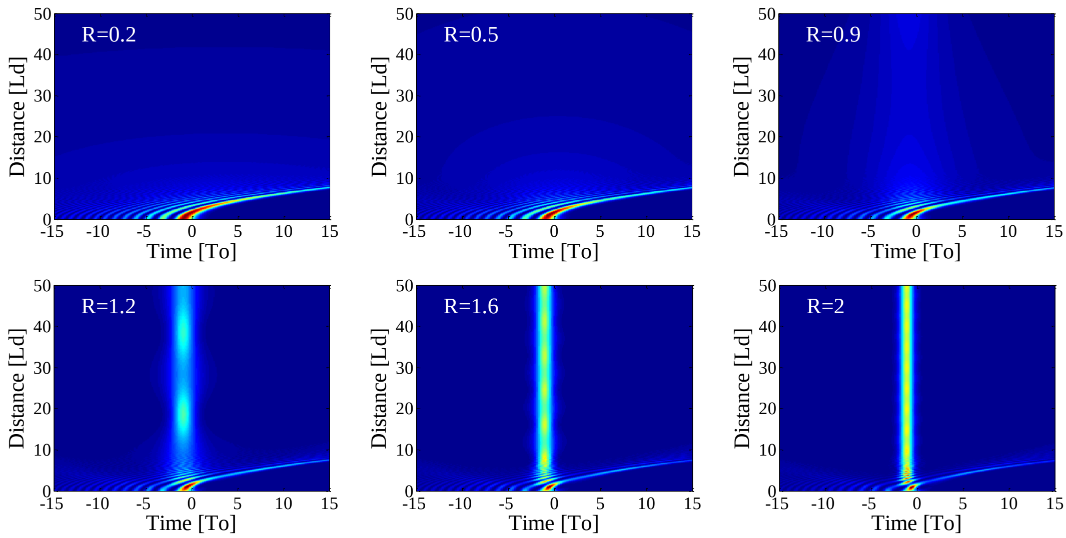

Figure 4.1– Propagation Images of truncated Airy pulse in nonlinear media for various launched power values.

The emergent soliton

Unsurprisingly, the shed pulse profile well conforms to a hyperbolic-secant function, or that of a soliton with background radiation. We fit a sech(·)+background radiation profile at every propagation distance and track the emergent soliton parameters.
Our fit model is

$$\left| A_0 \operatorname{sech}\left(\frac{T-T_p}{T_0}\right) + b \cdot e^{i\varphi(z)} \right|^2 = A_0^2 \operatorname{sech}^2\left(\frac{T-T_p}{T_0}\right) + b^2 + 2A_0 b \cos\left(\varphi(z)\right) \operatorname{sech}\left(\frac{T-T_p}{T_0}\right) \qquad \textbf{4.2}$$

This model is composed of the soliton intensity, the background radiation intensity and the interference between them. The parameter T_p describes the temporal position of the emergent soliton peak. Under the assumption that the oscillatory behavior of the emergent pulse is caused by the term $2A_0 b \cos\left(\varphi(z)\right) \operatorname{sech}\left(\frac{T-T_p}{T_0}\right)$ -the interference element- we set the magnitude of the soliton peak power to fixed value which determined by the mean value of the peak of the breathing pulse. The other parameters in the model, which describe the pulse width, the background radiation, the temporal position and the intensity of the interference element, are free in the fit process. After completing the fit process at every distance sample we got the variation of the pulse parameters along the propagation distance, which help us analyze the pulse and understand its evolution. Note that the oscillations of the time position, shown in Figure 4.4, are not noticeable without carrying out the fit process, due to the limited resolution of the numerical simulations.

The first step in the analysis is to verify that the emergent pulse is in fact a soliton. From Soliton theory we know that the formation of soliton requires that the following equilibrium condition

$$L_d = L_{NL} \Rightarrow P_0 T_0^2 = \frac{\beta_2}{\gamma} \qquad \textbf{4.3}$$

will be held.

According to the fit data, we find that the power × duration^2 product oscillates about this equilibrium condition (=1). These oscillations about the stable soliton condition verify that the pulse is indeed a soliton and they are known to arise as a result of interference between dispersive background radiation and the formed soliton [15] [16]. In figure 6.2 we can see the oscillations of this product for select R values. An interesting feature of this oscillation which is seen in the figure is that as *R* is larger, the mean value of the product is closer to 1- the ideal value.

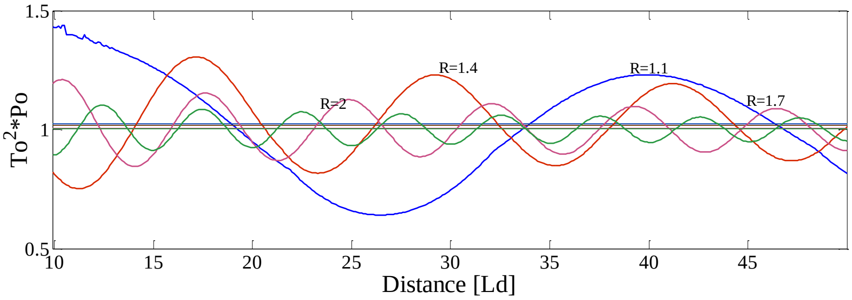

Figure 4.2- Evolution of soliton product along propagation distance for select R values together with their mean value.

We examined the relations between the soliton oscillations and the launched Airy peak power. In Figure 4.3(a) the oscillations of soliton width are shown as a function of propagation distance for select *R* values. The pulse width narrows and the oscillations period decreases with higher launch power. The decreasing oscillation period with increasing launch power is depicted in Figure 4.3(b). Similar behavior was reported in [17], where the amount of excess energy that was supplied to the launched soliton was expressed in the evolved soliton oscillations period. Another property of the oscillations is the modulation depth that sharply decreases with increased initial peak power (Figure 4.3(c)). We can relate the low modulation depth to the greater stability of the formed soliton and conclude that high launched peak power is required for stable soliton formation.

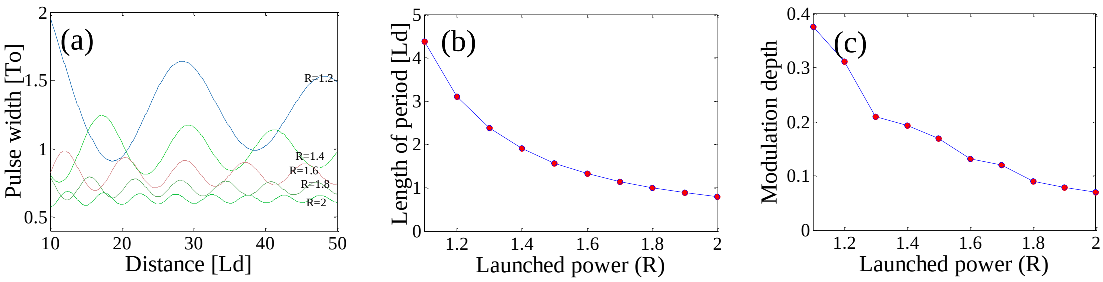

Figure 4.3 – (a) Oscillations of soliton width for different launched peak power, (b) soliton oscillations length of period as a function of launched peak power, (c) soliton oscillations modulation depth as a function of launched peak power.

Additional soliton parameters as soliton peak time position and phase also oscillate in similar manner as the peak power and width. Figure 4.4(a,c) shows the evolution of time position and phase as a function of propagation distance (phase fluctuations are plotted after subtracting the soliton's accumulated linear phase term). These oscillations are the result of interaction with the background radiation as explained in

[18] and demonstrated in [19] for the problem of background radiation that is formed by soliton amplification in optical communication.

From the results in Figure 4.4(a) we see that the position of the emergent soliton is also dependent on launch power. We plot the mean time position of the emergent soliton in Figure 4.4(b). More intense excitation results in the soliton appearing at an earlier time. This phenomena is explained by the fact that for low values of R a relatively long time is required for accumulation of enough energy by SPM for the soliton formation and shedding, and during this time the Airy pulse is accelerating and 'carries' the accumulating energy with it to later times. For larger R values there is enough energy in the Airy main lobe for soliton formation and shedding at an early point.

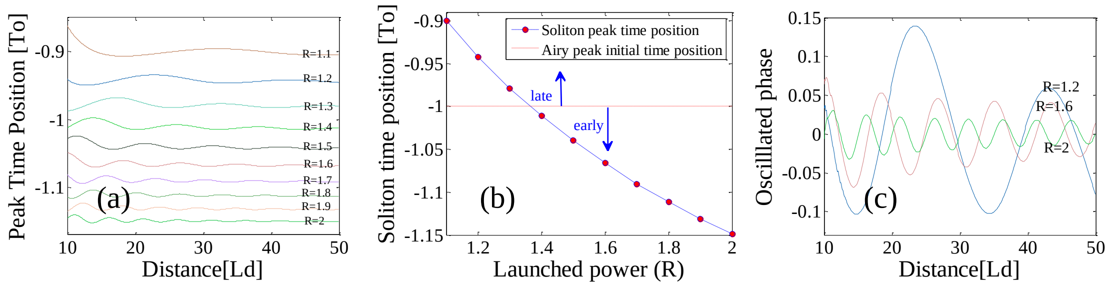

Figure 4.4– (a) Soliton peak time position along propagation distance, (b) mean soliton peak time position as a function of launched power. Note that Airy peak time position at launch is at t=-1. (c) soliton peak phase oscillations along propagation distance for select launched powers.

The accelerating wavefront

As seen in Figure 4.1, the Airy wavefront continues to exhibit the parabolic acceleration in time, even under the influence of Kerr effect and after shedding energy to the soliton. To study whether this acceleration continues with the properties of the linear propagation we compared the nonlinear propagations to linear, as the intensity is scaled with the R parameter. Note that the linear Airy pulse evolution is identical for every intensity value.

These linear propagation results are compared to the nonlinear ones by tracking the main lobe acceleration trajectory for each case and extracting information about its peak power and position. Furthermore, we calculate the accelerating energy distribution along propagation distance.

Figure 4.5 shows the Airy main lobe parabolic trajectory and peak power as a function of propagation distance, under linear and nonlinear propagation, for three select launched power cases. We see that the wavefront continues to exhibit the parabolic trajectory in time (blue curves), which is almost identical in the linear and the nonlinear propagation cases, although the nonlinear peak slightly trails the linear peak, on account of a delay associated with the energy shedding to the soliton. The intensity evolution of the accelerating wavefront is shown in green. We can see that in the nonlinear propagation its peak power performs decaying oscillations, as opposed to the monotonic decay in the linear case. The oscillations of the peak power in the nonlinear case are known to be a result of the interplay between the SPM and the dispersion. Similar influence of SPM on the Airy accelerating main lobe was already observed in [14]. However, the peak power oscillations there exhibit faster decay due to a relatively large truncation coefficient, 0.1-0.3 vs. 0.0335 in the current simulations.

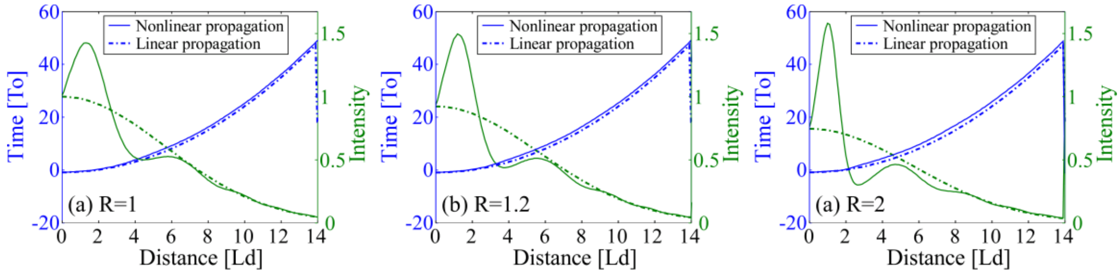

Figure 4.5 – Airy accelerating tail trajectories in time-distance space(blue) and in intensity-distance space (green) for (a) R=1, (b) R=1.2 and (c) R=2.

Next, we investigate the energy distribution of the accelerating wavefront. It is important to note that the simulations preserve the launched pulse energy along the propagation distance, as well as preservation of 'center of gravity' (first order moment) position according to the finite pulse energy and the uniformity of the media [4]. The power spectrum of the Airy pulse is symmetric about the central frequency, and upon propagation in anomalous dispersive media the high frequencies components are delayed (low frequency components are advanced) with respect to central frequency group delay (in anomalous media), such that the pulse total energy is eventually divided to two equal fractions about $T=0$- half of the energy at each direction. In the presence of Kerr nonlinearity, considerable part of the pulse energy is shed to the soliton that propagates at the group velocity, and the remaining energy disperses in opposite directions with less than a half of the launched energy dispersing to each side (due to soliton shedding).

The energy that is carried in the accelerating wavefront (delayed components) was found by summing the energy over positive time at every distance sample. These calculations were performed with both the linear and nonlinear propagations.

Figure 4.6(a) shows the delayed energy evolution of the accelerated Airy wavefront along the propagation distance for various Airy launched powers. The energy is normalized by the launched pulse energy, such that we can see the relative energy portion of the accelerating wavefront for linear and nonlinear cases. For all *R* values, the energy evolution of the linear propagations coincides to one curve that asymptotically approaches the value of half launched pulse energy, according to its linear nature. For the nonlinear propagations we clearly see that as *R* grows the fractional energy amount that is delayed is decreasing, where the oscillatory behavior is due to the soliton oscillations which take place in the boundary of the right half propagation plane. Those curves and those of Figure 4.6(b), which chart the energy evolution of the formed soliton for different *R* values, show the fact that the formed soliton not only has more intensity when *R* is growing, but also carries a larger energy fraction from the whole pulse. This can also be seen in Figure 4.6(c), where the mean soliton relative energy was calculated for every *R* value. From Figure 4.6(b-c) we also see the energy preservation—the normalized delayed energy is missing energy that is about half of the shed soliton energy, where the other half originates from the faster propagating energy components. When *R*=2, for example, the soliton energy fraction is about 0.39 and the missing fractional energy amount from the delayed energy is about 0.19, half of 0.39.

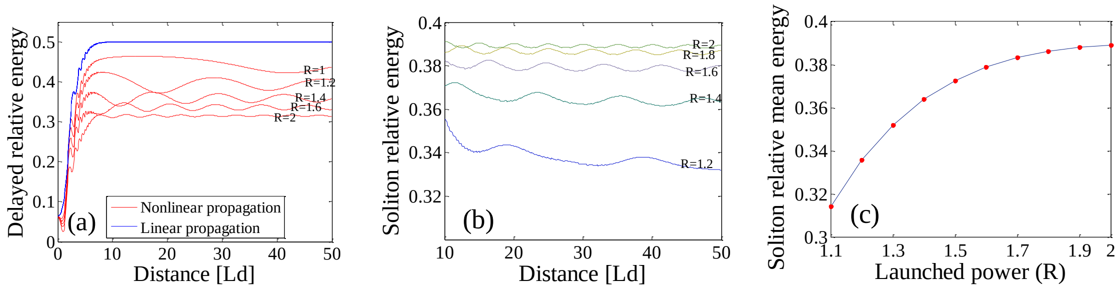

Figure 4.6 – (a) Airy tail relative energy for the linear and the nonlinear cases, (b) soliton relative energy, (c) soliton relative energy as function of launched power.

4.2 Truncation coefficient effect

The ability of Airy pulses to exhibit their unique features is strongly related to the degree of truncation in the apodization function. As the truncation is stronger, the Airy pulse quickly loses the unique features of the Airy pulse and disperses. Here we wish to examine how the truncation degree influences the soliton shedding and pulse propagation under the Kerr effect.

We employ the same pulse profile defined in Eq. (5.1), fixing the intensity scaling parameter *R* to 1.5 while varying the truncation coefficient in the range 0.01-0.1, as shown in Figure 1.6(a), and propagate the apodized Airy for every truncation value. Figure 4.7 shows examples of the Airy pulse evolution in time-distance space. We see that when the truncation is small the Airy original features as self-similarity and acceleration in time are more noticeable. The influence of the truncation degree on emergent soliton properties and on the accelerating wavefront was examined in the same manner as in the previous section.

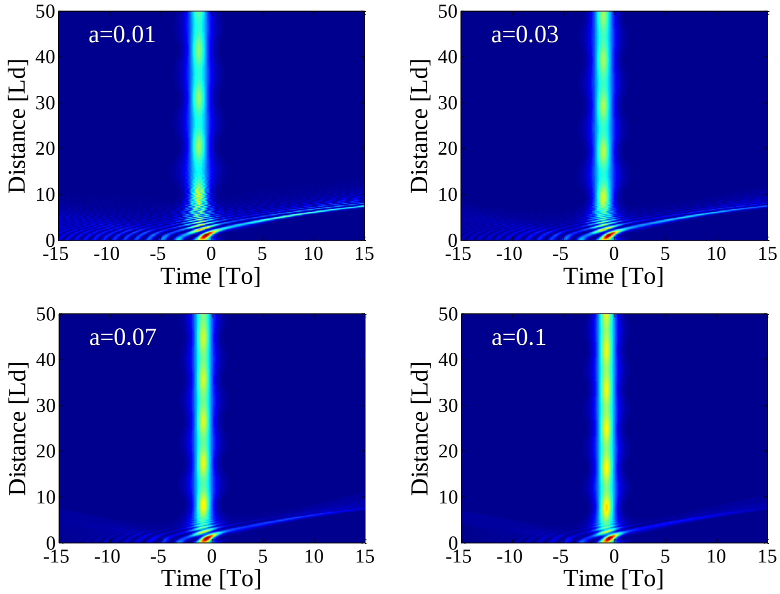

Figure 4.7 – propagation images of truncated Airy pulse in the nonlinear regime for various truncation values.

The emergent soliton

Larger truncation coefficient values make the exponential apodization of the Airy function stronger and the Airy tail is shortened; there is a negligible effect on the main Airy lobe, as shown in Figure 4.7(a). Hence the emergent soliton, which forms from the main lobe, achieves stability faster (after a shorter propagation distance) in cases of larger truncation coefficients, as the newly formed soliton experiences less collisions with the accelerating Airy tail, as shown in the propagation images in Figure 4.7. Therefore, the Sech(·) fit process was started from a different propagation distance for every truncation value.

From the soliton fit data we see that the emergent soliton parameters do not experience significant variations for different truncation values, as shown in the soliton parameters evolution curves in Figure 4.8(a-b). However, the soliton mean peak time position does shift considerably from the launched Airy peak position, and this shift increases for smaller truncation values (see Figure 4.8(c)). This behavior is explained by the interaction between the formed soliton from the main lobe and the accelerating lobes of the Airy tail, which constitute collision perturbations to the soliton and cause temporal shift of the soliton in the direction opposed to the accelerating lobes [20]. This temporal shift to earlier times depends on the perturbation energy, which increases for small truncation coefficient values. It is important to note that even without perturbing lobes, i.e. while propagating Airy with strong truncation (see Figure 4.9), the soliton is not necessarily formed at the launched Airy peak position because of the acceleration that the original pulse undergoes before the soliton is shed. Also, the launched Airy peak time position is not constant with different truncation coefficients (dashed red line in Figure 4.8(c)), as a result of a shift from the multiplication by the exponential apodization function.

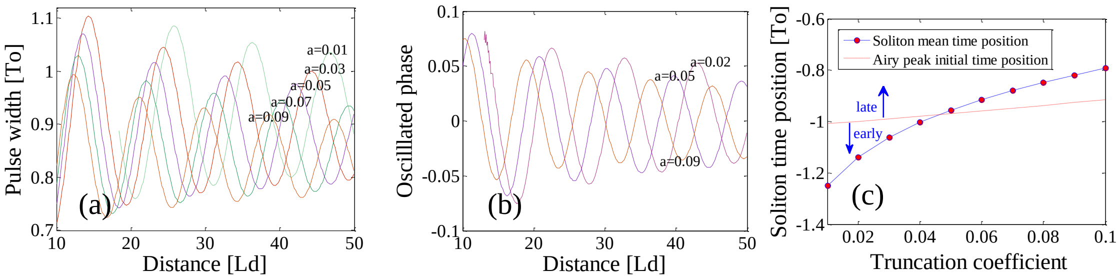

Figure 4.8 – Effect of different launched truncation values on oscillations of (a) soliton width and (b) soliton peak phase, (c) soliton peak time position as function of truncation coefficient. Note that Airy peak time position at launch is truncation value dependent, as evidenced by the dashed red line.

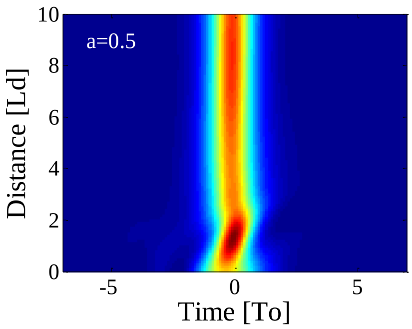

Figure 4.9- Propagation image of strongly truncated Airy pulse in the nonlinear regime. The temporal shift of the emergent soliton from the initial peak position is noticeable.

The accelerating wavefront

The extent to which the truncated Airy maintains its form and continues to accelerate before dispersing strongly depends on the truncation coefficient. As in the previous section, we compared the linear and the nonlinear propagations in order to investigate the Airy's accelerating wavefront behavior for different truncation values. In the linear propagation regime, the truncation coefficient determines both the distance at which the accelerating wavefront is still distinguishable, and the total Airy energy according to $E_{Airy} = (8\pi a)^{-1/2}$ [4]. In our investigation range for truncation coefficient, the linear Airy varies widely.

After tracking the accelerating wavefront trajectory for every truncation value, we compare the main lobe trajectory and peak power under the linear and the nonlinear propagation regimes (Figure 4.10). The main finding here is that the intensity of the accelerating main lobe in the nonlinear regime (green curves) first experiences SPM and focuses to the same peak power (with no dependence on truncation value). This peak is then shed to the soliton and the remaining accelerating wavefront immediately after the soliton shedding is at lower power compared to the linear propagation case. However, as a consequence of chromatic dispersion, the high frequency components travel slower and eventually the leading wavefront main lobe re-emerges and matches the main-lobe power of the linear propagation case (the Airy self-healing property). In spite of this wavefront matching between the linear and nonlinear propagations we see that in the nonlinear propagation the accelerating main lobe remains distinguishable for longer distances than in linear propagation for a given truncation value. This finding is related to the differences between the radiation energy distribution in the nonlinear and in the linear propagations. In the linear propagation (see example in Figure 1.6(b)) the dispersed Airy intensity roughly converges to a Gaussian distribution in time with propagation distance that eventually (after a certain distance) engulfs the accelerating main lobe. In the nonlinear propagation the dispersive radiation intensity is no longer Gaussian distributed due to the soliton formation and the energy centering about it, making the accelerating peak visible for longer propagation distance.

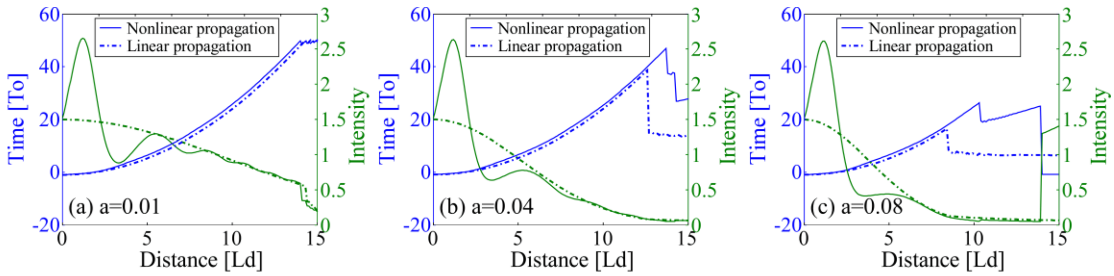

Figure 4.10 – Airy accelerating wavefront trajectories in time-distance space (blue) and in intensity-distance space (green) for (a) a=0.01, (b)a=0.04 and (c)a=0.08.

As the emergent soliton has roughly the same energy for all truncation values, its relative energy fraction in the launched pulse energy is larger for increasing truncation values (Figure 4.11(a)), therefore the relative energy fraction in the accelerating Airy wavefront decreases (Figure 4.11(b)). In the linear propagation regime the accelerating Airy energy always asymptotically approaches one half of the whole pulse energy, although its energy growth rate is truncation factor dependent. In the nonlinear case the delayed Airy energy fraction decreases from this value as the truncation is growing, as the nearly constant soliton energy is missing.

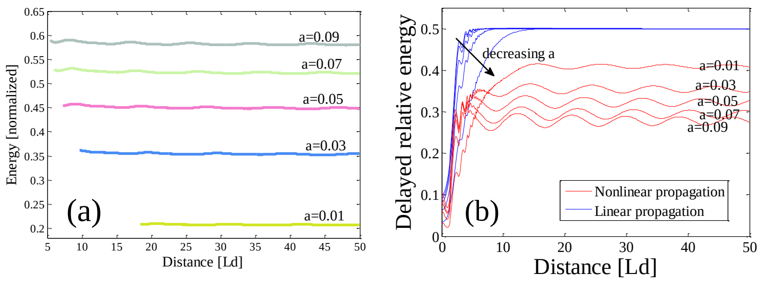

Figure 4.11 – Examples of energy evolution along propagation distance of (a) the relative energy of the emergent soliton (the soliton energy itself is hardly dependent on truncation coefficient) and (b) accelerating wavefront.

4.3 Soliton time position for power and truncation

In the previous sections we showed that: (1) the emergent soliton time position is at earlier times when the launched power increases (at fixed truncation) due to quicker build-up of a soliton. At lower powers, self-focusing results in the eventual build-up of the soliton, but as the conditions materialize the main lobe is undergoing the ballistic trajectory leading to soliton shedding at a later time position. The emergent soliton time position is at earlier times when the truncation coefficient decreases (at fixed launched power) due to collision perturbations with the accelerating tail lobes. The time shift associated with collision perturbations depends on the energy; hence higher truncation coefficients result in lower Airy tail energies and reduced soliton time shifts. These two effects are graphically depicted in Figure 4.12(a).

To verify that these two effects independently and consistently occur, we varied both the Airy launched power and the truncation coefficient over our investigation range (Figure 4.12 (b)). Indeed we see this trend continuing; the emergent soliton mean time position shifts to earlier (later) times for smaller (larger) truncation coefficients and for higher (lower) launched power levels. These results reinforce our finding that soliton is shed at an earlier time when the launched power is higher, and that collisions with the accelerating Airy tail lobes shift the position in the direction counter to the acceleration, i.e. towards earlier times.

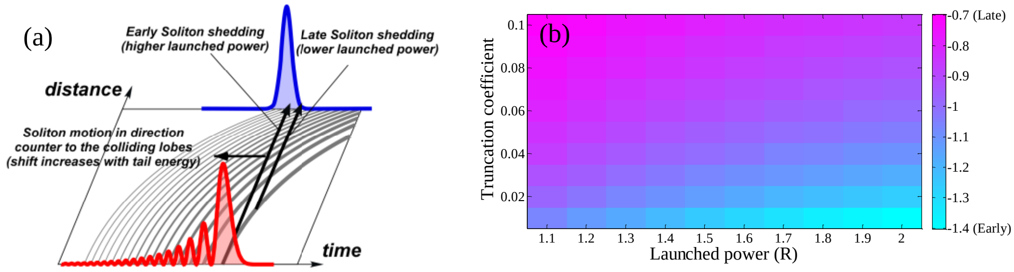

Figure 4.12 – (a) Schematic illustration of the sources of temporal shift of the emergent Soliton. (b) Distribution of Soliton mean time position as a function of truncation coefficient and launched power in our investigation range.

4.4 *Preliminary results of higher launched power Airy propagation*

By increasing the Airy launched power above *R=2* and simulating its propagation, we examined if there is any trend change in the breathing behavior of the emergent soliton. As in the main part of the research, the launched power was gradually increased with increments of 0.1 up to *R=3*. In Figure 4.13(a) we can see the soliton peak evolution along the propagation distance for various *R* values. It can be seen clearly that the trend of period length decreasing with increased launched power is maintained, which is explained by the fact that as the formed soliton peak power is higher it accumulates self-phase modulation faster and therefore the oscillations beating against the background radiation occur at higher rate- i.e. shortening of the oscillations period length. On the other hand, the modulation depth of the oscillations gets a minimal value when the launched power is around *R=2.7* and then it starts to increase again with the launched power. This finding is very surprising and intriguing, since this launched power value does not have any uniqueness apparently.

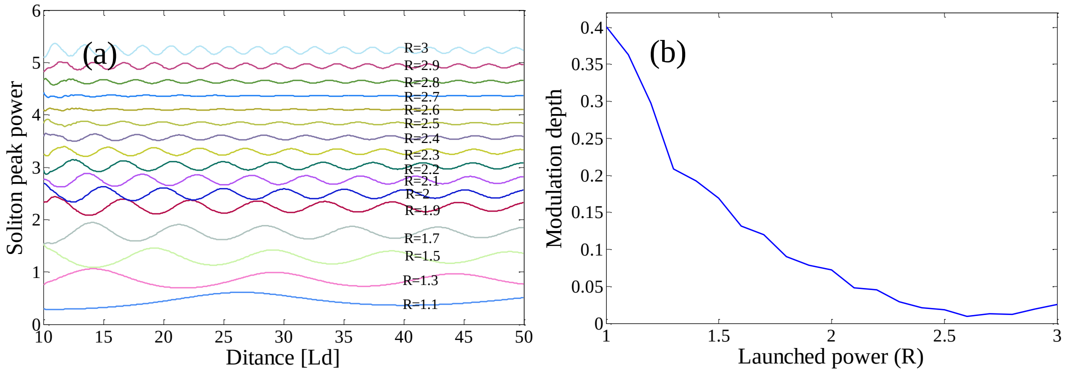

Figure 4.13- (a) Emergent soliton peak power oscillations along propagation distance for select R values. (b) Modulation depth of soliton oscillation as a function of extended launched power range.

Similar oscillatory results were shown in [17], where the launched pulse was a soliton with small gradually-changed excess energy and therefor it exhibits oscillatory behavior during propagation. The period length of the oscillations decreased with the launched power, but the minimal modulation depth of the soliton oscillations were obtained when the launched conditions of the propagation were the closest to the ideal soliton, i.e. when the perturbation was the smallest.

In our case, despite the fact that the initial conditions are always far from ideal soliton, we found the launch condition best matched to an unperturbed emergent soliton, exhibiting minimal modulation depth oscillations. We can assume from the mentioned research that in this situation the launched energy is divided perfectly to the soliton part and to the accelerating part, such that all the residual energy is diverted to the continuum, which is orthogonal to the soliton.

Trying explaining this phenomenon from the energy aspect, we compared the energy of the launched Airy pulse main lobe and the energy of the emergent soliton. The comparison results are shown in Figure 4.14. Despite our expectation to see relation between main lobe energy and emergent soliton stability (low modulation depth), these results do not explain the minimal modulation depth value at R=2.7, as we do not see a special relation between the launched Airy main lobe energy and the emergent soliton energy at this launched power value. An additional intriguing finding is that when R=2 the emergent soliton energy is the closest to the emergent soliton energy, but it cannot be explained by the known propagation properties of this launched power which was investigated and shown along this work.

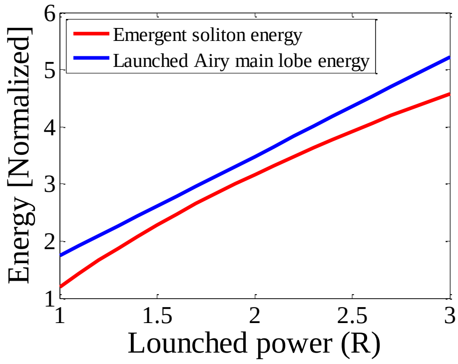

Figure 4.14 – Comparison between launched Airy main lobe energy and emergent soliton energy.

Extending of the Airy launched power range further is also expressed in shedding of two additional weaker solitary waves at both higher and lower center frequencies, as shown in the propagation image for R=4 in Figure 4.15.

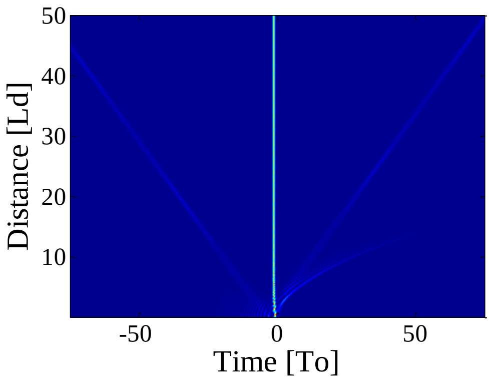

Figure 4.15 – Intensity distributions as a function of time and propagation distance for R=4, showing multiple soliton shedding at high launched peak powers.

These results should be investigated further in future work as well as the behavior of other parameters of the Airy pulse evolution in the extended power range.

5 Discussion and summary

In this research we investigated the propagation of a truncated temporal Airy pulse in nonlinear Kerr media. The phenomena of soliton shedding from the original Airy pulse under sufficiently strong excitation was already identified [11], but in this work we investigated in details the properties of the soliton and the remaining Airy radiation. We characterized the emergent soliton parameters under different truncation and power conditions and identified the mechanisms at play, in accordance to processes known from literature. The soliton parameters perform oscillations due to the presence of background radiation from the dispersed Airy pulse. The temporal position of the emergent soliton depends both on the Airy launched power and truncation coefficient, due to the location of the shedding event and the interaction with the accelerating Airy tail. We also observed the SPM influence on the accelerating Airy main lobe, and we found that the SPM has large effect on the accelerating main lobe visibility in comparison the linear truncated Airy propagation. Finally, we found that the energy distribution of the Airy pulse along the propagation depends on the launched power and the truncation degree.

We studied the soliton shedding phenomena for relatively intense launched Airy pulses that conform to the nonlinear Schrodinger equation (eq. 2.12) which is accurate for pulses of 5ps duration and longer. This research avenue can continue to even higher and shorter pulses, however eventually the well-understood phenomena explored here starts to break down. For proper simulation of short Airy pulse excitation, one should also add additional terms to account for higher-order nonlinear effects such as Raman scattering and self-steepening, and for the effect of third order dispersion.

6 References

[1] G. P Agrawal, *Nonlinear Fiber Optics*, University of Rochester, Rochester New York, 3th-ed.

[2] J. Durnin, “Exact solution for nondiffracting beams. I. The scalar theory,” J. Opt. Soc. Am. A 4, 651-654 (1987).

[3] M. V. Berry and N. L. Balazs, "Nonspreading Wave Packets," Am. J. Phys. 47, 264-267 (1979)

[4] G. A. Siviloglou, J. Broky, A. Dogariu, and D. N. Christodoulides, "Ballistic dynamics of Airy beams," Optics Letters **33**(3), 207-209 (2008).

[5] Jörg Baumgartl, Michael Mazilu and Kishan Dholakia, "Optically mediated particle clearing using Airy wavepackets," Nature Photonics 2, 675 - 678 (2008).

[6] Ido Dolev, Tal Ellenbogen, and Ady Arie, "Switching the acceleration direction of Airy beams by a nonlinear optical process," Optics Letters 35, 1581-1583 (2010)

[7] Pavel Polynkin, Miroslav Kolesik, Jerome V. Moloney, Georgios A. Siviloglou and Demetrios N. Christodoulides, " Curved Plasma Channel Generation Using Ultraintense Airy Beams," Science 10, 194-195 (2009).

[8] Pavel Polynkin, Miroslav Kolesik, and Jerome Moloney, "Filamentation of Femtosecond Laser Airy Beams in Water," Phys. Rev. Lett. **103**, 123902 (2009)

[9] Andy Chong, William H. Renninger, Demetrios N. Christodoulides and Frank W. Wise, "Airy–Bessel wave packets as versatile linear light bullets," Nature Photonics **4**, 103 - 106 (2010).

[10] Daryoush Abdollahpour, Sergiy Suntsov, Dimitrios G. Papazoglou, and Stelios Tzortzakis, "Spatiotemporal Airy Light Bullets in the Linear and Nonlinear Regimes," Phys. Rev. Lett. 105, 253901 (2010).

[11] C. Ament, P. Polynkin, and J. V. Moloney, "Supercontinuum Generation with Self-Healing Airy Pulses," in CLEO:2011 - Laser Applications to Photonic Applications, OSA Technical Digest (CD) (Optical Society of America, 2011), paper PDPC9.

[12] G. P Agrawal, *Fiber-Optic Communication Systems*, A John Wiley & Sons, Inc., Publication, 3th-ed, pp. 404-406

[13] J. Satsuma and N. Yajima, “Initial Value Problems of One-Dimensional Self-Modulation of Nonlinear Waves in Dispersive Media,” Prog. Theor. Phys. 55, 284 (1974).

[14] Rui-Pin Chen, Chau-Fu Yin, Xiu-Xiang Chu, Hui Wang, "Effect of Kerr Nonlinearity on an Airy Beam," Phys. Rev. A 82, 043832-043835, (2010).

[15] John Broky, Georgios A. Siviloglou, Aristide Dogariu, and Demetrios N. Christodoulides, "Self-healing properties of optical Airy beams," Optics Express **16**(17) ,12880-12891 (2008).

[16] N. Belanger and P. A. Belanger, "Bright solitons on a cw background," Optics Communications **124**, 301-308 (1996).

[17] Michel W Chbat, Paul R. Prucnal, Mohammed N. Islam, Carl E. Soccolich, and James P. Gordon, "Long-range interference effects of soliton reshaping in optical fibers," JOSA B **10**(8), 1386-1395 (1993).

[18] Akira Hasegawa and Yuji Kodama, "Amplification and reshaping of optical solitons in a glass fiber," Optics Letters, **7**(6), 285-287 (1982).

[19] E.A. Kuznetsov, A.V. Mikhailov, I.A. Shimokhin, "Nonlinear interaction of solitons and radiation," Physica D **87**, 201-215 (1995).

[20] Hermann A. Haus, Farzana I. Khatri, William S. Wong, Erich P. Ippen, and Kohichi R. Tamura, "Interaction of Soliton with Sinusoidal Wave Packet," Ieee Journal Of Quantum Electronics **32,** 917-924 (1996).

7 Appendix

7.1 Appendix A- Matlab code

Note: except for small variations, this Matlab code was written by Amitay Rudnick.

```
for R=0.1:0.1:3;

      % Pulse
      a=0.0335;
      k_p=0.286895-0.58008*a+ 0.756411*a^2;%Normalization factor for
      peak power according to the truncation coefficient
      PoAiry=R/k_p;%A Different offset is  required for different
      values of the truncation coefficent.
      To_Airy=1;
      AoAiry=sqrt(PoAiry);%Peak Amplitude Airy

      %Fiber
      beta2=-1; %Fiber quadratic dispersion coefficent [sec^2/Km].
      beta3=0; %Third order dispersion coefficent[sec^3/Km].
      gamma=1; %Fiber nonlinear coefficent [1/Km*W].
      alpha=0; %fiber loss coefficent,gain=alph<0[1/Km].

      % Length scales definitions.

      Ld=(To_Airy^2)/abs(beta2) ;%Dispersion distance [Km].
      Lnl=1/(gamma*R);%Nonlinear distance [Km].
      Ld_beta3=To_Airy^3/abs(beta3); % Dispersion distance third order
      [Km].

      if Ld>Ld_beta3;
          Ld=Ld_beta3;
      end

      %Program definitions
      P_D=50*Ld; %Propagation Distance acording Kilomters.
      Samples_D=500;%The number of samples along the distance.
      Increment=P_D/Samples_D;
      sigma=To_Airy/sqrt(2);
      beta_RC=0.01; % Beta factor for the raised cosine window.
      Time_Factor_Dispersion=25;
      %Flags
      Flag_Time_Window='on';
      Window_Time_Shift=200;

      % Chossing time window size.
      %if Ld<=Lnl;

      Tstop=round(Time_Factor_Dispersion*(sqrt(1+(P_D*beta2/(sigma^2*2
      ))^2+(1/2)*(beta3*P_D/(4*sigma^3))^2))*sigma-Window_Time_Shift);
      %Dispersion propagation.
      Tstart= round(-
      Time_Factor_Dispersion*(sqrt(1+(P_D*beta2/(sigma^2*2))^2+(1/2)*(
      beta3*P_D/(4*sigma^3))^2))*sigma-Window_Time_Shift);
```

```
clear sigma
%Program definitions (continued)
Tres=0.1;

Z=0:Increment:P_D; %Creation of the distance Array.
T=Tstart:Tres:Tstop-Tres; %Creation of the time array
Wres=2*pi/(Tstop-Tstart);% Angular frequency resolution
W=Wres*(-length(T)/2:1:(length(T)/2-1));%Angular frequency
array.


% Choosing propagation constant.
if min(Ld,Lnl)<=P_D
    if Increment<=min(Ld,Lnl)/1000
        h=Increment;
    else Increment>min(Ld,Lnl)/1000;
        K=ceil(Increment/(min(Ld,Lnl)/1000));
        h=Increment/K;
    end
else min(Ld,Lnl)>P_D;
    h=Increment;
end

clear K

%  Time window function
if strcmp(Flag_Time_Window,'on')

      Number_Of_Indices_For_Window=length(T); %Window Size
      Raised_cosine =zeros(1,length(T));
      Start_Position_Raised_cosine=(length(T)-
      Number_Of_Indices_For_Window)/2+1;

      Stop_Position_Raised_cosine=Number_Of_Indices_For_Window+S
      tart_Position_Raised_cosine-1;

      Raised_cosine(Start_Position_Raised_cosine:Stop_Position_R
      aised_cosine)=tukeywin(Number_Of_Indices_For_Window,beta_R
      C)';

End

U_in=AoAiry*airy(T/To_Airy).*exp((T/To_Airy)*a)
Aw=Tres*fftshift(fft(fftshift(U_in)));


Propagated_Pulse_Time_Domain_Matrix=zeros(length(Z),length(T));%
saving the pulse data after every increment
Propagated_Pulse_Frequency_Domain_Matrix=zeros(length(Z),length(
W));
Energy_Of_Pulse=zeros(length(Z),1);
Array_Counter=1;


for Dis_Counter=0:Increment:P_D; % Distance in Kilometers,data
saved at the end of each intervals.

                % Split-Step propagation between intervals.
```

```
                    for Dis_SS_Counter=h:h:Increment

                        case 'off'

                            Aw=Aw.*exp(-
alpha/2*(h/2)+i*(beta2/2)*W.^2*(h/2)-i*(beta3/6)*W.^3*(h/2));
%Dispersion propagation effects.
                            A=ifft(fftshift(Aw))/Tres;
                            A=fftshift(A);
                            A=A.*exp(i*gamma*((abs(A)).^2)*(h));
%Nonlinear propagation effects.
                            Aw=Tres*fftshift(fft(fftshift(A)));
                            Aw=Aw.*exp(-
alpha/2*(h/2)+i*(beta2/2)*W.^2*(h/2)-i*(beta3/6)*W.^3*(h/2));
%Dispersion propagation effects.

                        case 'on'

                            Aw=Aw.*exp(-
alpha/2*(h/2)+i*(beta2/2)*W.^2*(h/2)-i*(beta3/6)*W.^3*(h/2));
%Dispersion propagation effects.
                            A=ifft(fftshift(Aw))/Tres;
                            A=fftshift(A);
                            A=A.*exp(i*gamma*((abs(A)).^2)*(h));
%Nonlinear propagation effects.
                            A=A.*Raised_cosine;
                            Aw=Tres*fftshift(fft(fftshift(A)));
                            Aw=Aw.*exp(-
alpha/2*(h/2)+i*(beta2/2)*W.^2*(h/2)-i*(beta3/6)*W.^3*(h/2));
%Dispersion propagation effects.

                    end

                end % End split step increments

A=ifft((fftshift(Aw)))/Tres; % Inverse Fourier transform.
A=fftshift(A);

Propagated_Pulse_Time_Domain_Matrix(Array_Counter,:)=A; %
saving of the output pulsein the time domain.
Propagated_Pulse_Frequency_Domain_Matrix(Array_Counter,:)=Aw;%
saving on the output pulse in the frequency domain.
% Energy calculation for each step.

Energy_Increment=trapz((abs(A)).^2)*Tres;

Energy_Of_Pulse(Array_Counter)=Energy_Increment;

Array_Counter=Array_Counter+1;

waitbar(Dis_Counter/P_D);

end %End of propagation to distance (P_D).

end
```

7.2 Appendix B- published paper

The paper can be find in the URL

http://www.opticsinfobase.org/oe/abstract.cfm?uri=oe-19-18-17298

Citation:

Yiska Fattal, Amitay Rudnick, and Dan M. Marom, "Soliton shedding from Airy pulses in Kerr media," Opt. Express **19**, 17298-17307 (2011)

Soliton shedding from Airy pulses in Kerr media

Yiska Fattal,* Amitay Rudnick, and Dan M. Marom

Department of applied physics, Hebrew University, Givat Ram, Jerusalem 91904, Israel
*yiska.fatal@mail.huji.ac.il

Abstract: We simulate and analyze the propagation of truncated temporal Airy pulses in a single mode fiber in the presence of self-phase modulation and anomalous dispersion as a function of the launched Airy power and truncation coefficient. Soliton pulse shedding is observed, where the emergent soliton parameters depend on the launched Airy pulse characteristics. The Soliton temporal position shifts to earlier times with higher launched powers due to an earlier shedding event and with greater energy in the Airy tail due to collisions with the accelerating lobes. In spite of the Airy energy loss to the shed Soliton, the Airy pulse continues to exhibit the unique property of acceleration in time and the main lobe recovers from the energy loss (healing property of Airy waveforms).

OCIS codes: (190.0190) Nonlinear optics; (190.3270) Kerr effect; (060.5530) Pulse propagation and temporal solitons.

References and links

1. M. V. Berry and N. L. Balazs, “Nonspreading wave packets,” Am. J. Phys. **47**(3), 264–267 (1979).
2. G. A. Siviloglou, J. Broky, A. Dogariu, and D. N. Christodoulides, “Ballistic dynamics of Airy beams,” Opt. Lett. **33**(3), 207–209 (2008).
3. J. Baumgartl, M. Mazilu, and K. Dholakia, “Optically mediated particle clearing using Airy wavepackets,” Nat. Photonics **2**(11), 675–678 (2008).
4. I. Dolev, T. Ellenbogen, and A. Arie, “Switching the acceleration direction of Airy beams by a nonlinear optical process,” Opt. Lett. **35**(10), 1581–1583 (2010).
5. P. Polynkin, M. Kolesik, J. V. Moloney, G. A. Siviloglou, and D. N. Christodoulides, “Curved plasma channel generation using ultraintense Airy beams,” Science **324**(5924), 229–232 (2009).
6. P. Polynkin, M. Kolesik, and J. Moloney, “Filamentation of femtosecond laser Airy beams in water,” Phys. Rev. Lett. **103**(12), 123902 (2009).
7. A. Chong, W. H. Renninger, D. N. Christodoulides, and F. W. Wise, “Airy–Bessel wave packets as versatile linear light bullets,” Nat. Photonics **4**(2), 103–106 (2010).
8. D. Abdollahpour, S. Suntsov, D. G. Papazoglou, and S. Tzortzakis, “Spatiotemporal airy light bullets in the linear and nonlinear regimes,” Phys. Rev. Lett. **105**(25), 253901 (2010).
9. C. Ament, P. Polynkin, and J. V. Moloney, “Supercontinuum generation with self-healing Airy pulses,” in CLEO:2011—Laser Applications to Photonic Applications, OSA Technical Digest (CD) (Optical Society of America, 2011), paper PDPC9.
10. R.-P. Chen, C.-F. Yin, X.-X. Chu, and H. Wang, “Effect of Kerr nonlinearity on an Airy beam,” Phys. Rev. A **82**(4), 043832–043835 (2010).
11. N. Belanger and P. A. Belanger, “Bright solitons on a cw background,” Opt. Commun. **124**(3-4), 301–308 (1996).
12. M. W. Chbat, P. R. Prucnal, M. N. Islam, C. E. Soccolich, and J. P. Gordon, “Long-range interference effects of soliton reshaping in optical fibers,” J. Opt. Soc. Am. B **10**(8), 1386–1395 (1993).
13. A. Hasegawa and Y. Kodama, “Amplification and reshaping of optical solitons in a glass fiber-I,” Opt. Lett. **7**(6), 285–287 (1982).
14. E. A. Kuznetsov, A. V. Mikhailov, and I. A. Shimokhin, “Nonlinear interaction of solitons and radiation,” Physica D **87**(1-4), 201–215 (1995).
15. H. A. Haus, F. I. Khatri, W. S. Wong, E. P. Ippen, and K. R. Tamura, “Interaction of soliton with sinusoidal wave packet,” IEEE J. Quantum Electron. **32**(6), 917–924 (1996).
16. G. P. Agrawal, *Nonlinear Fiber Optics* (Academic Press, 2001).
17. J. Broky, G. A. Siviloglou, A. Dogariu, and D. N. Christodoulides, “Self-healing properties of optical Airy beams,” Opt. Express **16**(17), 12880–12891 (2008).

#148647 - $15.00 USD Received 2 Jun 2011; revised 5 Aug 2011; accepted 12 Aug 2011; published 18 Aug 2011

1. Introduction

Airy pulses [1], whose electric field temporal profile is defined by an Airy function which is a one-sided, oscillating function having infinite energy, are a solution to the linear dispersion equation

$$i\frac{\partial A}{\partial z}=\frac{\beta_2}{2}\frac{\partial^2 A}{\partial T^2}, \tag{1}$$

and exhibit two interesting features: during propagation the waveform maintains its shape in the presence of dispersion and its wavefront accelerates in time (or travels along a ballistic trajectory) in a time frame moving at the group velocity. However, true Airy pulses are impractical as they contain an infinite amount of energy. By apodizing the Airy pulse, i.e. truncating the semi-infinite oscillations, in our case with a decaying exponential envelope, the waveform maintains its two unique properties over an extended propagation range despite its finite energy (Fig. 1(a)) [2]. Truncated Airy pulses occur naturally if a Gaussian pulse is propagated in a fiber at the zero dispersion point, under the influence of cubic dispersion.

In complete analogy to the Airy pulse solution to the dispersion Eq. (1), spatial Airy beams are a solution to the paraxial equation. Spatial Airy beams have been investigated extensively in the last few years, and found to be useful for various applications such as optical micromanipulation [3], optical switching [4], plasma channel generation [5], and laser filamentation [6]. More recently, temporal Airy pulses are being investigated, in the context of spatiotemporal light bullets in linear conditions [7] and in nonlinear conditions [8], and in the context of one dimensional Airy pulse propagation, under the influence of strong nonlinearity giving rise to supercontinuum and solitary wave generation [9].

In this study, we analyze temporal Airy pulse propagation in media exhibiting Kerr nonlinearity as occurring in single mode silica fibers, leading to the phenomena of self-phase modulation (SPM) and anomalous dispersion. The influence of the Kerr nonlinear effect on spatial Airy beams was investigated under relatively weak parameters and transient narrowing of the Airy main lobe—caused by SPM—was observed [10]; however, we are interested in operating under much higher intensities where the nonlinear effect results in soliton shedding from the Airy pulse and not just a small perturbation of the Airy beam. Although we analyze temporal Airy pulse propagation in fiber, our results are also valid for spatial Airy beams diffracting in Kerr media on account of the isomorphism between the dispersion Eq. (1) and the paraxial diffraction equation.

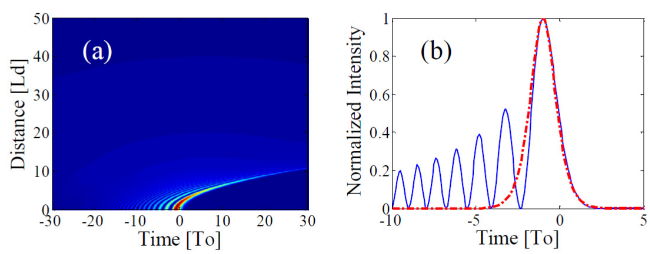

Fig. 1. (a) Intensity distribution as a function of time and propagation distance for truncated Airy pulse in the linear regime (or low launch power). (b) Launched Airy pulse in time (blue solid curve), compared to a soliton pulse (red dashed curve).

The evolution of light pulses in single-mode dispersive-nonlinear medium is governed by the Nonlinear Schrödinger Equation (NLSE),

$$i\frac{\partial A}{\partial z}=\frac{\beta_2}{2}\frac{\partial^2 A}{\partial T^2}-\gamma\left|A\right|^2 A \tag{2}$$

where β_2 is the dispersion coefficient, γ is the nonlinear coefficient and A is the wave amplitude that depends on local time-T, and distance-z. Due to the addition of the nonlinear

#148647 - $15.00 USD Received 2 Jun 2011; revised 5 Aug 2011; accepted 12 Aug 2011; published 18 Aug 2011

potential (or SPM term) in the NLSE, the Airy function is no longer a valid solution and we cannot predict analytically the Airy pulse evolution. The Soliton, on the other hand, is a well-known solution of the NLSE. For the canonical first order case, its profile is $\sqrt{P_0}\,\mathrm{Sech}(t/T_0)\cdot\mathrm{Exp}(iz\beta_2/T_0^{\,2})$, where P_0 is peak power and T_0 is duration and it is obtained only when there is equilibrium between the dispersion and the nonlinear effect, leading to the condition

$$P_0\cdot T_0^{\,2}=\frac{|\beta_2|}{\gamma}. \tag{3}$$

The soliton then maintains its form and power level, provided no losses are present. Cases of perturbed soliton propagation (i.e. when there are small deviations from the condition set in Eq. (3) were extensively investigated [11–15], which help us interpret the emergent soliton behavior in our simulations.

In this paper, we propagate Airy pulses with different intensities and apodization values and investigate both the resulting ‘emergent soliton’ parameters, as well as the behavior of the residual Airy pulse. All our simulations are based on numerical solutions of the NLSE, using the split-step Fourier method (SSFM). This numerical method was chosen due to its efficiency in simulating one-dimensional pulse propagation [16].

1.1. Normalization terms

In our simulations we used the normalized NLSE form [16]

$$i\frac{\partial A}{\partial z}=\mathrm{sgn}(\beta_2)\frac{1}{2}\frac{\partial^2 A}{\partial T^2}-|A|^2A, \tag{4}$$

where $|\beta_2| = \gamma = T_0 = 1$, and the launched Airy pulse profile is defined as:

$$A(T,z{=}0)=\sqrt{R\cdot K_p(a)}\cdot\mathrm{Ai}(T)\cdot\mathrm{Exp}(a\cdot T) \tag{5}$$

where 0‹a«1 is the truncation coefficient, and $K_p(a)$ is a truncation-dependent factor that sets the pulse peak intensity to 1 for any a value . This factor was numerically calculated and found to be in parabolic dependence with the truncation coefficient. T is the time variable in a frame of reference that moves with the wave group velocity, i.e. $T=t-z/v_g$, and R is a dimensionless parameter we vary for scaling the Airy power. At R=1 the Airy main lobe intensity profile looks quite similar to the fundamental soliton, as shown in Fig. 1(b).

We measure the propagation distance in L_d units, defined as $L_d=T_0^2/\beta_2$, which in our normalized coordinates equals 1.

2. Effects of launched Airy power

In order to investigate the influence of Airy launched power on its evolution, we varied the scaling parameter R in the range 0.1-2 and for every R value we propagated the pulse using the SSFM algorithm. Figure 2 shows pulse evolution examples for select R values. At low launched power, the Airy pulse performs the acceleration in time and subsequently it succumbs to dispersion. However, when R is sufficiently large (above 0.9) a stationary soliton pulse is formed out of the centered energy about the Airy main lobe. The soliton exhibits periodic oscillations in the soliton amplitude and width as a function of propagation distance. In addition, we witness the resilience of the temporal Airy waveform to shedding of a fraction of the energy as a soliton; the wavefront continues to propagate along a parabolic trajectory. Similar resilience has been shown in main lobe masking for spatial Airy beams [17] and in supercontinuum generation for temporal Airy pulses propagation [9].

#148647 - $15.00 USD Received 2 Jun 2011; revised 5 Aug 2011; accepted 12 Aug 2011; published 18 Aug 2011

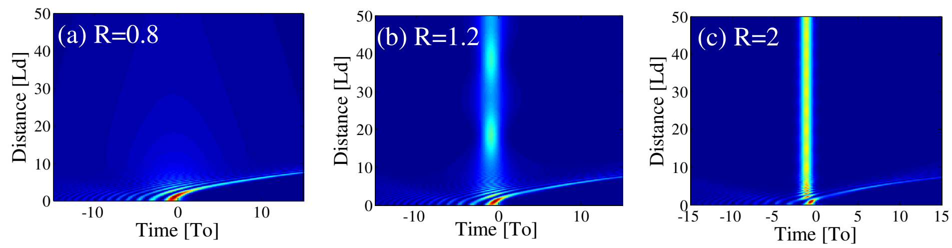

Fig. 2. Intensity distributions as a function of time and propagation distance in the nonlinear propagation regime for: (a) $R = 0.8$, (b) $R = 1.2$, and (c) $R = 2$.

2.1. *The emergent soliton*

Unsurprisingly, the shed pulse profile well conforms to a hyperbolic-secant function, or that of a soliton with background radiation. We fit a sech(·) + background radiation profile at every propagation distance and track the emergent soliton peak power, duration and time position along the propagation distance. We find that the power × duration^2 product oscillates about the equilibrium condition (= 1) defined in Eq. (2). These oscillations about the stable soliton are known to arise as a result of interference between dispersive background radiation and the formed soliton [11,12].

We examined the relations between the soliton oscillations and the launched Airy peak power. In Fig. 3(a) the oscillations of soliton width are shown as a function of propagation distance for select R values. The pulse width narrows and the oscillations period decreases with higher launch power. The decreasing oscillation period with increasing launch power is depicted in Fig. 3(b). Similar behavior was reported in [12], where the amount of excess energy that was supplied to the launched soliton was expressed in the evolved soliton oscillations period. Another property of the oscillations is the modulation depth that sharply decreases with increased initial peak power (Fig. 3(c)). We can relate the low modulation depth to the greater stability of the formed soliton and conclude that high launched peak power is required for stable soliton formation.

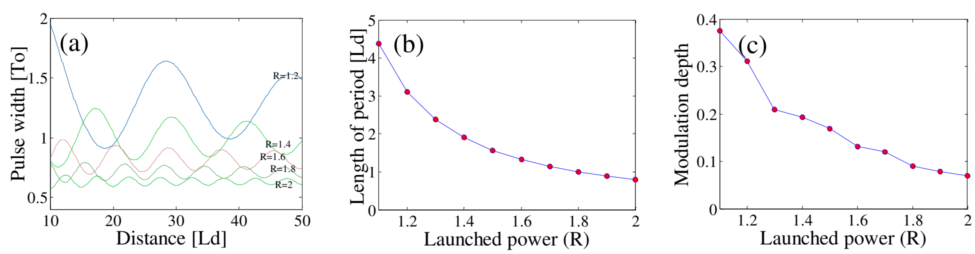

Fig. 3. (a) Oscillations of soliton width for different launched peak power, (b) soliton oscillations length of period as a function of launched peak power, (c) soliton oscillations modulation depth as a function of launched peak power.

Additional soliton parameters as soliton peak time position and phase also oscillate in similar manner as the peak power and width. Figures 4(a, c) show the evolution of time position and phase as a function of propagation distance (phase fluctuations are plotted after subtracting the soliton's accumulated linear phase term). These oscillations are the result of interaction with the background radiation as explained in [13] and demonstrated in [14] for the problem of background radiation that is formed by soliton amplification in optical communication.

From the results in Fig. 4(a) we see that the position of the emergent soliton is also dependent on launch power. We plot the mean time position of the emergent soliton in Fig. 4(b). More intense excitation results in the soliton appearing at an earlier time. This phenomena is explained by the fact that for low values of R a relatively long time is required

#148647 - $15.00 USD Received 2 Jun 2011; revised 5 Aug 2011; accepted 12 Aug 2011; published 18 Aug 2011

for accumulation of enough energy by SPM for the soliton formation and shedding, and during this time the Airy pulse is accelerating and 'carries' the accumulating energy with it to later times. For larger R values there is enough energy in the Airy main lobe for soliton formation and shedding at an early point.

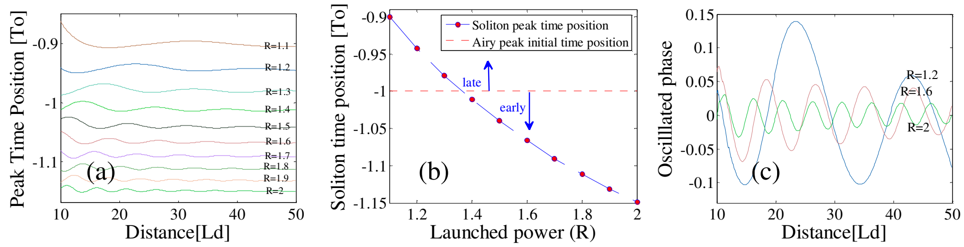

Fig. 4. (a) Soliton peak time position along propagation distance, (b) mean soliton peak time position as a function of launched power. Note that Airy peak time position at launch is at t = −1. (c) soliton peak phase oscillations along propagation distance for select launched powers.

2.2. The accelerating wavefront

As seen in Fig. 2, the Airy wavefront continues to exhibit the parabolic acceleration in time, even under the influence of Kerr effect and after shedding energy to the soliton. To study whether this acceleration continues with the properties of the linear propagation we compared the nonlinear propagations to linear, as the intensity is scaled with the R parameter. Note that the linear Airy pulse evolution is identical for every intensity value.

These linear propagation results are compared to the nonlinear ones by tracking the main lobe acceleration trajectory for each case and extracting information about its peak power and position. Furthermore, we calculate the accelerating energy distribution along propagation distance.

Figure 5 shows the Airy main lobe parabolic trajectory and peak power as a function of propagation distance, under linear and nonlinear propagation, for three select launched power cases. We see that the wavefront continues to exhibit the parabolic trajectory in time (blue curves), which is almost identical in the linear and the nonlinear propagation cases, although the nonlinear peak slightly trails the linear peak, on account of a delay associated with the energy shedding to the soliton. The intensity evolution of the accelerating wavefront is shown in green. We can see that in the nonlinear propagation its peak power performs decaying oscillations, as opposed to the monotonic decay in the linear case. The oscillations of the peak power in the nonlinear case are known to be a result of the interplay between the SPM and the dispersion. Similar influence of SPM on the Airy accelerating main lobe was already observed in [10]. However, the peak power oscillations there exhibit faster decay due to a relatively large truncation coefficient, 0.1-0.3 vs. 0.0335 in the current simulations.

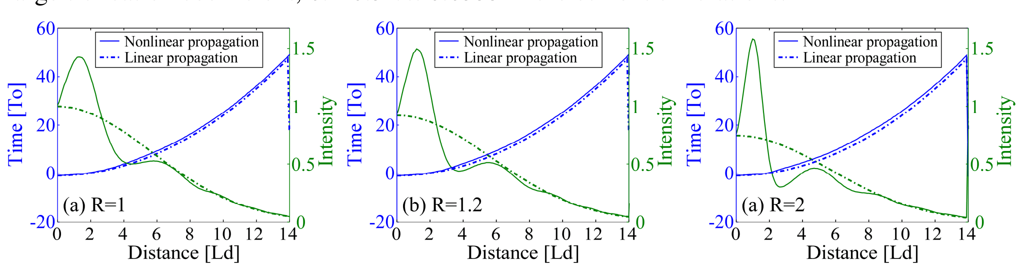

Fig. 5. – Airy accelerating tail trajectories in time-distance space(blue) and in intensity-distance space (green) for (a) R = 1, (b) R = 1.3 and (c) R = 2.

Next, we investigate the energy distribution of the accelerating wavefront. It is important to note that the simulations preserve the launched pulse energy along the propagation distance, as well as preservation of 'center of gravity' (first order moment) position according to the finite pulse energy and the uniformity of the media [2]. The power spectrum of the Airy pulse is symmetric about the central frequency, and upon propagation in anomalous dispersive media the high frequencies components are delayed (low frequency components are advanced) with respect to central frequency group delay (in anomalous media), such that the pulse total energy is eventually divided to two equal fractions about T = 0- half of the energy at each direction. In the presence of Kerr nonlinearity, considerable part of the pulse energy is shed to the soliton that propagates at the group velocity, and the remaining energy disperses in opposite directions with less than a half of the launched energy dispersing to each side (due to soliton shedding).

The energy that is carried in the accelerating wavefront (delayed components) was found by summing the energy over positive time at every distance sample. These calculations were performed with both the linear and nonlinear propagations.

Figure 6(a) shows the delayed energy evolution of the accelerated Airy wavefront along the propagation distance for various Airy launched powers. The energy is normalized by the launched pulse energy, such that we can see the relative energy portion of the accelerating wavefront for linear and nonlinear cases. For all R values, the energy evolution of the linear propagations coincides to one curve that asymptotically approaches the value of half launched pulse energy, according to its linear nature. For the nonlinear propagations we clearly see that as R grows the fractional energy amount that is delayed is decreasing, where the oscillatory behavior is due to the soliton oscillations which take place in the boundary of the right half propagation plane. Those curves and those of Fig. 6(b), which chart the energy evolution of the formed soliton for different R values, show the fact that the formed soliton not only has more intensity when R is growing, but also carries a larger energy fraction from the whole pulse. This can also be seen in Fig. 6(c), where the mean soliton relative energy was calculated for every R value. From Figs. 6(b-c) we also see the energy preservation—the normalized delayed energy is missing energy that is about half of the shed soliton energy, where the other half originates from the faster propagating energy components. When R = 2, for example, the soliton energy fraction is about 0.39 and the missing fractional energy amount from the delayed energy is about 0.19, half of 0.39.

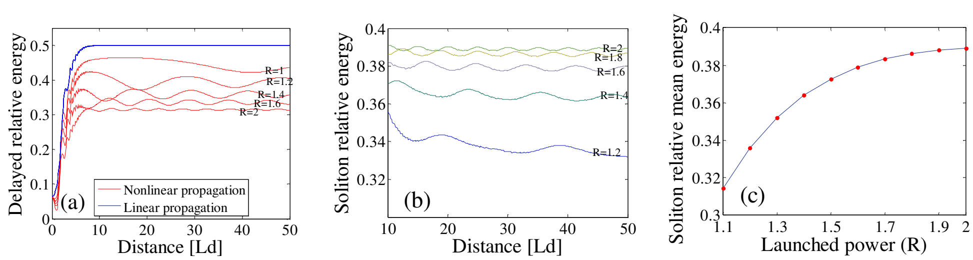

Fig. 6. (a) Airy tail relative energy for the linear and the nonlinear cases, (b) soliton relative energy, (c) soliton relative energy as function of launched power.

3. Truncation coefficient effect

The ability of Airy pulses to exhibit their unique features is strongly related to the degree of truncation in the apodization function. As the truncation is stronger, the Airy pulse quickly loses the unique features of the Airy pulse and disperses. Here we wish to examine how the truncation degree influences the soliton shedding and pulse propagation under the Kerr effect.

We employ the same pulse profile defined in Eq. (4), fixing the intensity scaling parameter R to 1.5 while varying the truncation coefficient in the range 0.01-0.1, as shown in Fig. 7(a), and propagate the apodized Airy for every truncation value. Figures 7(b-c) show two examples of the Airy pulse evolution in time-distance space. We see that when the truncation is small the Airy original features as self-similarity and acceleration in time are more noticeable. The influence of the truncation degree on emergent soliton properties and on the accelerating wavefront was examined in the same manner as in the previous section.

#148647 - $15.00 USD Received 2 Jun 2011; revised 5 Aug 2011; accepted 12 Aug 2011; published 18 Aug 2011

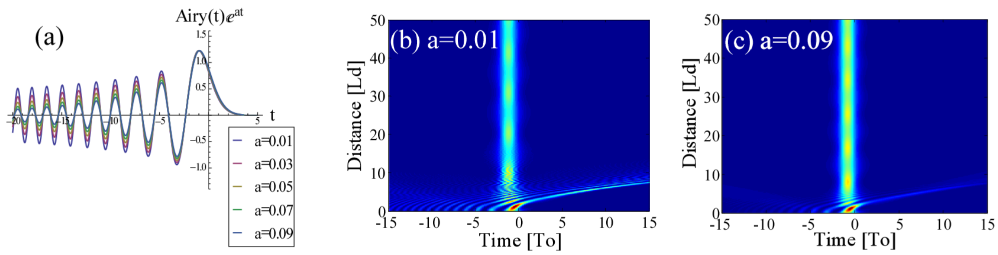

Fig. 7. (a) Launched Airy amplitude for several truncation values, (b)-(c) Intensity distributions as a function of time and propagation distance for: (b) a = 0.01, (c) a = 0.09.

3.1. *The emergent soliton*

Larger truncation coefficient values make the exponential apodization of the Airy function stronger and the Airy tail is shortened; there is a negligible effect on the main Airy lobe, as shown in Fig. 7(a). Hence the emergent soliton, which forms from the main lobe, achieves stability faster (after a shorter propagation distance) in cases of larger truncation coefficients, as the newly formed soliton experiences less collisions with the accelerating Airy tail, as shown in the propagation images in Fig. 7. Therefore, the Sech(•) fit process was started from a different propagation distance for every truncation value.

From the soliton fit data we see that the emergent soliton parameters do not experience significant variations for different truncation values, as shown in the soliton parameters evolution curves in Figs. 8(a-b). However, the soliton mean peak time position does shift considerably from the launched Airy peak position, and this shift increases for smaller truncation values (see Fig. 8(c)). This behavior is explained by the interaction between the formed soliton from the main lobe and the accelerating lobes of the Airy tail, which constitute collision perturbations to the soliton and cause temporal shift of the soliton in the direction opposed to the accelerating lobes [15]. This temporal shift to earlier times depends on the perturbation energy, which increases for small truncation coefficient values. It is important to note that even without perturbing lobes (i.e. while propagating Airy with strong truncation), the soliton is not necessarily formed at the launched Airy peak position because of the acceleration that the original pulse undergoes before the soliton is shed. Also, the launched Airy peak time position is not constant with different truncation coefficients (dashed red line in Fig. 8(c)), as a result of a shift from the multiplication by the exponential apodization function.

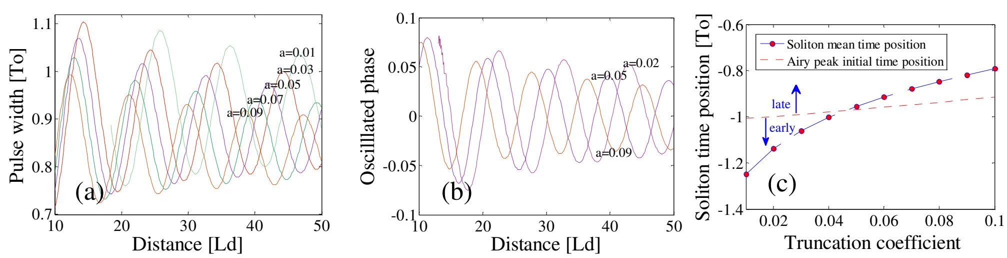

Fig. 8. Effect of different launched truncation values on oscillations of (a) soliton width and (b) soliton peak phase, (c) soliton peak time position as function of truncation coefficient. Note that Airy peak time position at launch is truncation value dependent, as evidenced by the dashed red line.

3.2. *The accelerating wavefront*

The extent to which the truncated Airy maintains its form and continues to accelerate before dispersing strongly depends on the truncation coefficient. As in the previous section, we compared the linear and the nonlinear propagations in order to investigate the Airy's accelerating wavefront behavior for different truncation values. In the linear propagation regime, the truncation coefficient determines both the distance at which the accelerating wavefront is still distinguishable, and the total Airy energy according to $E_{Airy} = (8\pi a)^{-1/2}$ [2]. In our investigation range for truncation coefficient, the linear Airy varies widely.

After tracking the accelerating wavefront trajectory for every truncation value, we compare the main lobe trajectory and peak power under the linear and the nonlinear propagation regimes (Fig. 9). The main finding here is that the intensity of the accelerating main lobe in the nonlinear regime (green curves) first experiences SPM and focuses to the same peak power (with no dependence on truncation value). This peak is then shed to the soliton and the remaining accelerating wavefront immediately after the soliton shedding is at lower power compared to the linear propagation case. However, as a consequence of chromatic dispersion, the high frequency components travel slower and eventually the leading wavefront main lobe re-emerges and matches the main-lobe power of the linear propagation case (the Airy self-healing property). In spite of this wavefront matching between the linear and nonlinear propagations we see that in the nonlinear propagation the accelerating main lobe remains distinguishable for longer distances than in linear propagation for a given truncation value. This finding is related to the differences between the radiation energy distribution in the nonlinear and in the linear propagations. In the linear propagation (see example in Fig. 1(a)) the dispersed Airy intensity roughly converges to a Gaussian distribution in time with propagation distance that eventually (after a certain distance) engulfs the accelerating main lobe. In the nonlinear propagation the dispersive radiation intensity is no longer Gaussian distributed due to the soliton formation and the energy centering about it, making the accelerating peak visible for longer propagation distance.

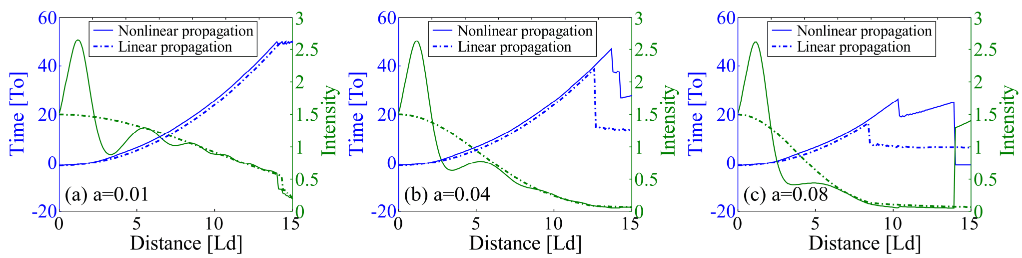

Fig. 9. Airy accelerating wavefront trajectories in time-distance space (blue) and in intensity-distance space (green) for (a) a = 0.01, (b)a = 0.04 and (c)a = 0.08.

As the emergent soliton has roughly the same energy for all truncation values, its relative energy fraction in the launched pulse energy is larger for increasing truncation values (Fig. 10(a)), therefore the relative energy fraction in the accelerating Airy wavefront decreases (Fig. 10(b)) In the linear propagation regime the accelerating Airy energy always asymptotically approaches one half of the whole pulse energy, although its energy growth rate is truncation factor dependent. In the nonlinear case the delayed Airy energy fraction decreases from this value as the truncation is growing, as the nearly constant soliton energy is missing.

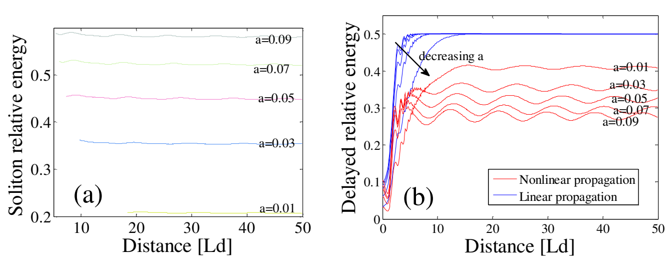

Fig. 10. Examples of energy evolution along propagation distance of (a) the relative energy of the emergent soliton (the soliton energy itself is hardly dependent on truncation coefficient) and (b) accelerating wavefront.

4. Soliton time position for power and truncation

In the previous sections we showed that: (1) the emergent soliton time position is at earlier times when the launched power increases (at fixed truncation) due to quick build-up of a soliton. At lower powers, self-focusing results in the eventual build-up of the soliton, but as the conditions materialize the main lobe is undergoing the ballistic trajectory leading to soliton shedding at a later time position. And (2) the emergent soliton time position is at earlier times when the truncation coefficient decreases (at fixed launched power) due to collision perturbations with the accelerating tail lobes. The time shift associated with collision perturbations depends on the energy; hence higher truncation coefficients result in lower Airy tail energies and reduced soliton time shifts. These two effects are graphically depicted in Fig. 11(a).

To verify that these two effects independently and consistently occur, we varied both the Airy launched power and the truncation coefficient over our investigation range (Fig, 11(b)). Indeed we see this trend continuing; the emergent soliton mean time position shifts to earlier (later) times for smaller (larger) truncation coefficients and for higher (lower) launched power levels. These results reinforce our finding that soliton is shed at an earlier time when the launched power is higher, and that collisions with the accelerating Airy tail lobes shift the position in the direction counter to the acceleration, i.e. towards earlier times.

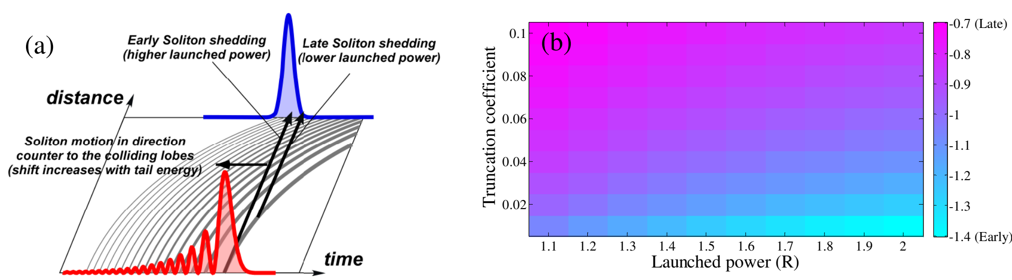

Fig. 11. (a) Schematic illustration of the sources of temporal shift of the emergent Soliton. (b) Distribution of Soliton mean time position as a function of truncation coefficient and launched power in our investigation range.

5. Summary

In this paper we investigated the propagation of a truncated temporal Airy pulse in nonlinear Kerr media. The phenomena of soliton shedding from the original Airy pulse under sufficiently strong excitation was already identified [8,9], but in this work we investigated in detail the properties of the soliton and the remaining Airy radiation. We characterized the emergent soliton parameters under different truncation and power conditions and identified the mechanisms at play, in accordance to processes known from literature. The soliton parameters perform oscillations due to the presence of background radiation from the dispersed Airy pulse. The temporal position of the emergent soliton depends both on the Airy launched power and truncation coefficient, due to the location of the shedding event and the interaction with the accelerating Airy tail. We also observed the SPM influence on the accelerating Airy main lobe, and we found that the SPM has large effect on the accelerating main lobe visibility in comparison the linear truncated Airy propagation. Finally, we found that the energy distribution of the Airy pulse along the propagation depends on the launched power and the truncation degree.

In this work we studied the soliton shedding phenomena for relatively intense launched Airy pulses. This research avenue can continue to even higher launched pulse powers, however eventually the well-understood phenomena explored here starts to break down. Figure 12 shows the time-space evolution when launching the Airy pulse with a power factor of four (R = 4). We see that for such intense excitation three solitons are shed, the main soliton in a consistent manner to that described here, and two additional weaker soliton s at

#148647 - $15.00 USD Received 2 Jun 2011; revised 5 Aug 2011; accepted 12 Aug 2011; published 18 Aug 2011

both higher and lower center frequencies. This result was still obtained with the standard nonlinear Schrodinger equation (Eq. (4)). However, for proper simulation of intense Airy pulse excitation, one should also add additional terms to account for higher-order nonlinear effects such as Raman scattering and self-steepening.

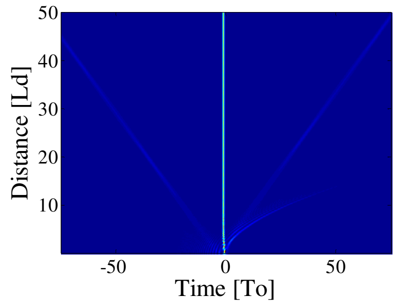

Fig. 12. Intensity distributions as a function of time and propagation distance for R = 4, showing multiple soliton shedding at high launched peak powers.

#148647 - $15.00 USD Received 2 Jun 2011; revised 5 Aug 2011; accepted 12 Aug 2011; published 18 Aug 2011

ממצא חשוב בהתפתחות פולס האיירי בתווך לא ליניארי הוא שלמרות אובדן האנרגיה לטובת יצירת סוליטון, האיירי ממשיך להציג את המאפיין הייחודי של ההאצה בזמן של חלק מהאנרגיה ובנוסף אנחנו רואים כי האונה הראשית של הפולס, שתרמה את מרבית האנרגיה ליצירת הסוליטון, משחזרת את עצמה- מה שמוכר כ"תכונת הריפוי העצמי של האיירי"- ומבצעת את התנועה הבליסטית המוכרת מהתחום הליניארי כאשר עוצמתה מתנודדת עד שדועכת כתוצאה מיחסי גומלין בין הדיספרסיה לבין תופעת אפנון הפאזה העצמי.

בנוסף לבדיקת השפעת האי-ליניאריות על התפתחות הפולס, נחקרת ג"כ השפעת רמת הקטימה של פולס האיירי המשוגר על התפתחותו יחד עם השפעת התופעה הלא ליניארית. אנו מוצאים כי עבור רמת קטימה נמוכה- כלומר הגדלת האנרגיה שנושא הפולס ב"זנב" שלו- האונות המשניות של פולס האיירי המרכיבות את הזנב המאיץ הופכות להיות יותר דומיננטיות, דבר שיש לו השפעה ניכרת על המרחק שעובר הפולס על לאירוע פליטת הסוליטון, על המיקום הזמני שלו- כתוצאה מהתנגשויות עם אונות הזנב המאיצות משתנה המיקום הזמני בהתאם לכמות האנרגיה שהן נושאות איתן, ועל כמות האנרגיה המאיצה במערכת לעומת כמות האנרגיה הנעה במהירות קבועה בצורת סוליטון.

תקציר

פולס מסוג "איירי", שהצורה הפונקציונלית שלו היא פתרון של משוואת הדיספרסיה, מפגין 2 תכונות ייחודיות: האחת- שמירה על פרופיל זמני קבוע במהלך ההתקדמות בתווך דיספרסיבי, והשנייה היא היכולת להאיץ (ולהאט) בזמן- כלומר לנוע לאורך מסלול פרבולי בתוך חלון זמן הנע יחד עם הפולס במהירות החבורה המאפיינת אותו.

תכונות אלו התגלו לראשונה בהקשר של מכניקה קוונטית כמאפיינות תנועת חלקיק חופשי במרחב מאחר ופונקציית איירי מהווה פתרון של משוואת שרדינגר לחלקיק חופשי. לאחרונה הוצגו תוצאות תיאורטיות וניסיוניות המוכיחות כי לתכונות אלו יש ביטוי גם בתחום קרני האור לאור הדמיון בין משוואת שרדינגר לחלקיק חופשי לבין משוואת הדיפרקציה המתארת התקדמות אלומת אור בתווך ולבין משוואת הדיספרסיה המתארת התקדמות של פולס זמני בתווך ליניארי (דיספרסיבי).

אמנם, פולס איירי "אמיתי" אינו בר מימוש בשל האנרגיה האינסופית שהוא נושא עימו אולם קטימת האנרגיה באמצעות הכפלה בפונקציה מעריכית מאפשרת את מימושו של פולס איירי כמעט "אמיתי" ששומר על תכונותיו הייחודיות לאורך מרחק ניכר- ביחס לפולסים מסוגים אחרים- אך לבסוף סובל מהשפעת הדיפרקציה/דיספרסיה ודועך.

בעבודה זו אנו חוקרים את ההשפעה של תכונת האי-ליניאריות של תווך כדוגמת סיב אופטי- המתבטאת ב"אפנון פאזה עצמי" (SPM)- על ההתקדמות וההתפתחות של פולס איירי קטום. עבור עוצמות נמוכות, כאשר התופעות הלא ליניאריות לא באות לידי ביטוי ניתן לנבא בצורה אנליטית את התפתחות הפולס בכל נקודת זמן ובכל מרחק התקדמות, אולם כאשר מגדילים את העוצמה ההתחלתית של הפולס התופעה הלא ליניארית מתחילה להשפיע וצורת ההתקדמות המוכרת אינה מתקיימת בהכרח.

ע"י הגברה הדרגתית של עוצמת פולס האיירי המשוגר למערכת אנו בוחנים את השפעת העוצמה- ובעצם את השפעת האי-ליניאריות- על התפתחות הפולס. אנו מוצאים כי עבור עוצמת שיגור מספיק גדולה, פולס מסוג סוליטון נפלט מתוך פולס האיירי כאשר הפרמטרים של הסוליטון הנפלט תלויים במאפייני פולס האיירי המשוגר. הסוליטון מבצע "נשימות" במהלך ההתקדמות בסיב- כלומר ישנה השתנות מחזורית של הפרמטרים של הסוליטון כתוצאה מיחסי גומלין עם קרינת הרקע. קרינת הרקע נובעת משארית אנרגית האיירי שלא השתתפה בתהליך יצירת הסוליטון ובמקום זאת התפתחה כמו איירי ליניארי ולבסוף עברה דיספרסיה. המחזוריות של הנשימות גדלה עם הגברת עוצמת האור המשוגרת אך רמת האפנון שלה (עומק המודולציה) קטנה כאשר העוצמה גדלה. הגדלה נוספת של עוצמת הפולס המשוגר מגלה כי ישנה עוצמת שיגור עבורה רמת האפנון היא מינימלית ומעבר לה היא עוברת למגמת עליה, בעוד מגמת העליה במחזוריות הפולס נותרת בעינה.

מאפיין נוסף של הסוליטון הנפלט המושפע מהעוצמה ההתחלתית של האיירי הוא המיקום הזמני (הממוצע) של הסוליטון, הנע לזמן יותר מוקדם ככל שעוצמת השיגור גדלה, עקב צבירת אנרגיה מספקת לפליטת הסוליטון כבר בשלב מוקדם בהתפתחות הפולס בעוצמות היותר גבוהות.

תודות

בראש ובראשונה תודה לדן, על ההנחיה המסורה ועל התמיכה לאורך כל התקופה.
תודה לחברי הקבוצה במעבדה להתקנים פוטוניים שהיו שם בכל שאלה והתייעצות.
תודה ליואל, אישי היקר, על שתמך, המריץ ועודד ללא הרף.

תודה לאלוקים, שהוא הנותן לנו כֹח לעשות חיל.

האוניברסיטה העברית בירושלים

הפקולטה למדעי הטבע

המחלקה לפיזיקה יישומית

פליטת סוליטון מתוך פולס מסוג איירי בתווך

לא ליניארי בעל אפקט קר

מגישה: יסכה פתאל

021682554

מנחה: ד"ר דן מרום

עבודת גמר לתואר מוסמך במדעי הטבע

תאריך הגשה: אייר תשע"ב